EURAS JOURNAL of Engineering and Applied Sciences

EURAS JOURNAL OF ENGINEERING AND APPLIED SCIENCES

Volume 2 Issue 2 2022

General DOI: 10.17932/EJEAS.2021.024
Volume 2 Issue 2 DOI: 10.17932/EJEAS.2021.024/2022.202

EURAS JOURNAL OF ENGINEERING AND APPLIED SCIENCES

ISSN : 2757-7961

Language
English

Publication Period
Published issues per year: February, August

Volume 2 Issue 2 - August 2022

Correspondence Addres
EJEAS - EURAS JOURNAL OF ENGINEERING AND APPLIED SCIENCES
Adress: Beşyol Mah. İnönü Cad. No: 38 İstanbul - Türkiye
Phone: +90 (212) 411 61 68
E-mail: euras@euras-edu.org

Printed by
Levent Baskı Merkezi
Sertifika No: 35983
Emniyetevler Mahallesi Yeniçeri Sokak No:6/A
4.Levent / İstanbul, Türkiye
Tel: 0212 270 80 70
E-mail: info@leventbaskimerkezi.com

Editorial Board

Scientific Advisory Board

Contents

Research Article

DOI Numbers

General DOI: 10.17932/EJEAS.2021.024
Volume 2 Issue 2 DOI: 10.17932/EJEAS.2021.024/2022.202

Foundation Design Analysis with Finite Element Method in the Reinforcement of Liquid Storage Tanks
Mehmet Fatih ALTAN, Hakkıcan ALÇAN
10.17932/EJEAS.2021.024/ejeas_v02i2001

Using Deep Learning on System Identification of the Retaining Wall Model
Sertaç TUHTA
10.17932/EJEAS.2021.024/ejeas_v02i2002

Covıd-19 Faqs Chatbot Using Artificial Neural Network with Bag of Words
Abdelrahman R. S. ALMASSRI, Nour AMMAR, Ufuk Fatih KÜÇÜKALI
10.17932/EJEAS.2021.024/ejeas_v02i2003

Design and Thrust/Weight Optimization of a Supersonic Plug Nozzle by Truncation
Sıdalı HAIF, Hakım KBAB, Amına BENKHEDDA
10.17932/EJEAS.2021.024/ejeas_v02i2004

Numerical Analysis on Heat Transfer and Flow Characteristic Through Elliptical Twisted Tube
Toygun DAĞDEVİR
10.17932/EJEAS.2021.024/ejeas_v02i2005

From The Editor

Euras Journal of Engineering and Applied Sciences (EJEAS), is a peer-reviewed academic journal, establishing a solid platform for all academicians, consultants, researchers, and those who have a strong interest in global current issues and trends in engineering and applied sciences. Euras Journal of Engineering and Applied Sciences is based on engineering and applied sciences; artificial intelligence, cybersecurity, environmental sciences, food and food safety, biotechnology, material science and composites, nanotechnology, energy technologies, electronics, robotics, thermal sciences, earthquakes – structures – foundation and earth sciences studies. Subject areas could be as narrow as a specific phenomenon or device or as broad as a system.

EJEAS was established with the intention of promoting scholarly communication all over the world in a more effective manner. Our aim is to establish a publication that will be abstracted and indexed in the Engineering Index (EI) and Science Citation Index (SCI) in the near future. The journal has a short processing period to encourage young scientists.

Prof. Dr. Hasan HEPERKAN
Editor

Research Article

FOUNDATION DESIGN ANALYSIS WITH FINITE ELEMENT METHOD IN THE REINFORCEMENT OF LIQUID STORAGE TANKS

Mehmet Fatih ALTAN[1], Hakkıcan ALÇAN[2]

[1]Prof. Dr. at Department of Civil Engineering, Istanbul Arel University, Istanbul, mehmetfatihaltan@arel.edu.tr

[2]Department of Civil Engineering, Istanbul Aydin University, Istanbul, hakkicanalcan@stu.aydin.edu.tr
ORCID: 0000-0002-1329-61760000-0002-1329-6176

ABSTRACT

The calculation tables created for the liquid storage tank examined in this study cover the design of the tank foundation. The soil bearing capacity was checked according to the allowable stress design d and the settlement-swelling potential was evaluated. The geometry of the ring foundation wall proposed for reinforcement is an inverted T-section rotating around the tank diameter. In this context, the model ring wall was analyzed for each load case using the finite element method with the SAP2000 software. In this study, a different solution method was proposed to transfer the seismic load to the foundation, and only the induction of the seismic shear force at the center of gravity of the tank was sufficient to design the ring circumferential foundation. This force was transferred to the ring wall by hypothetical rigid members, and then computer software multiplied the shear force by the loading distance to generate the seismic moment. Therefore, there is no need to use both seismic moment and shear in the basic model of the liquid storage tank. In the study, the results related to stability control and anchor design are given in detail.

Keywords: *Foundation Reinforcement, Settlement Calculations, Finite Element Method, Stability.*

Received: 12.02.2022 - Accepted: 02.06.2022
DOI: 10.17932/EJEAS.2021.024/ejeas_v02i2001

1. INTRODUCTION

The calculation tables created for the storage tank examined in the study cover the design of the tank foundation. The reinforced concrete structure was designed in accordance with the latest design method using the Turkish standard and the cement type was selected according to the geotechnical report. Soil bearing capacity was checked according to the allowable stress design method (Elastic Design Requirement) and soil parameters were taken from a geotechnical survey. The allowable bearing capacity is given as 270 kN/m^2. Thus, the soil strain constant Ks is estimated to be equal to 37500 kN/m^3. The basic geometry of the ring wall is an inverted T-section rotating in the Z-axis around a tank diameter of 19.00 m. The inverted T-section has a flange 500 mm thick and 3000 mm wide. The connecting plate is 1500 mm high and 700 mm thick. The tank design provides the input loads applied to the ring wall foundation. This download is used for the design of the ring wall and related controls requested from the relevant codes.

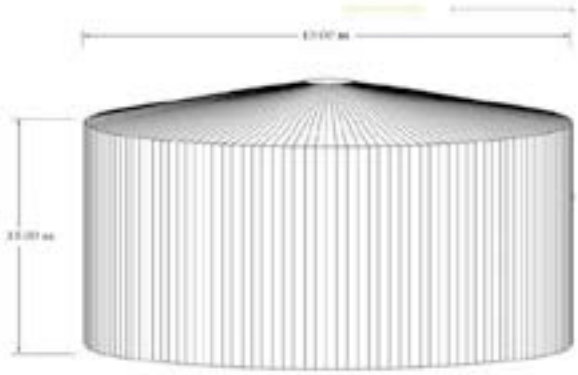

Figure 1: Dimensions of liquid storage tank

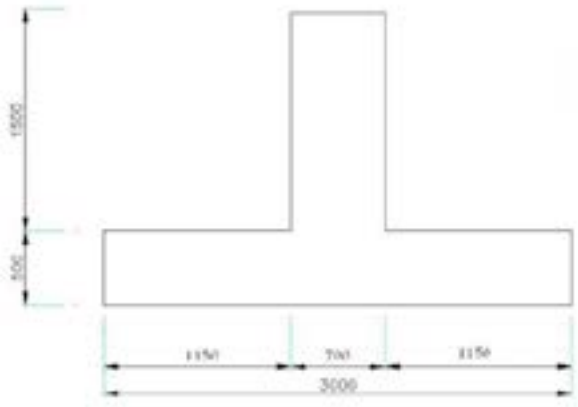

Figure 2: Dimension of foundation

The springs are applied to the foundation mat, and the software calculates the relevant spring constant automatically. The average size of the finite element mesh is 0.50 m. Concrete grade C30 and reinforcement steel grade St 420.

Table 1: Equipment data and general assumptions

Physical quantities	Value	Unit	Statement
C.L.D.	*19*	*m*	*Mechanical data*
f_c	*300*	*kg/cm²*	*Assumption*
f_y	*4200*	*kg/cm²*	*Assumption*
Seismic shear	*1182,00*	*ton/m²*	*Mechanical data*
G_S	*2*	*ton/m²*	*Basic geotechnical investigation*
Maximum liquid level	*18*	*m*	*Mechanical data*
Allowable soil bearing pressure	*27*	*ton/m²*	*Basic geotechnical investigation*
Area	*283,52*	*m*	*Calculated*
G_L	*1*	*ton/m²*	*Mechanical data*

Loads considered to act upon the tank are dead, lifeve, operating, test load\ and operating condition earthquake.

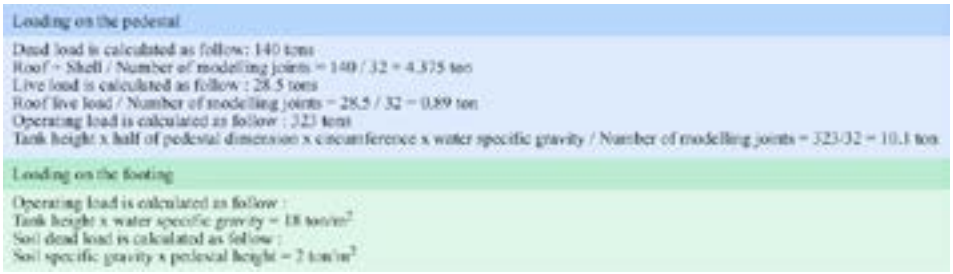

Figure 3: Loading

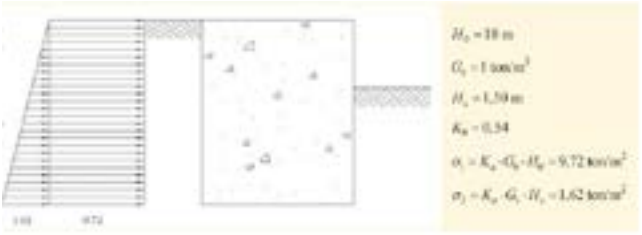

Figure 4: Calculation of soil lateral pressure

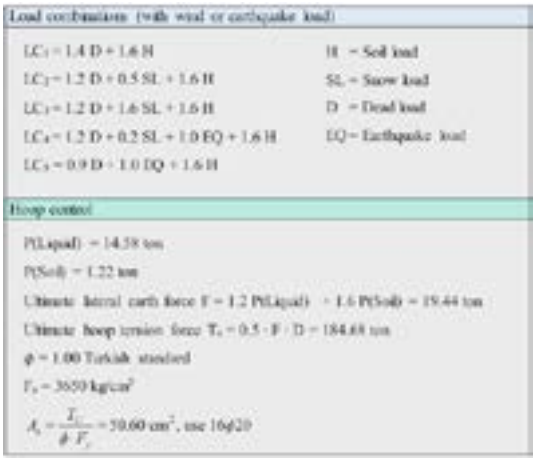

Figure 5: Design of foundation

2. FINITE ELEMENT ANALYSIS OF LIQUID STORAGE TANK

The empty space is the rigid zone under the ring wall foundation. The values of bending moments should be considered outside of this zone which means just on both sides of the ring wall. Pink section lines were taken into account for reinforcement and the rigid zone was excluded.

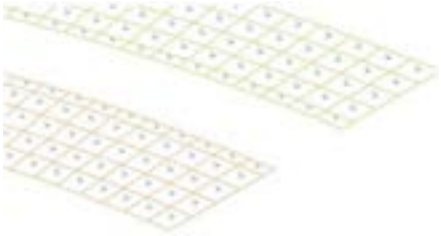

Figure 6: Area under ring wall foundation

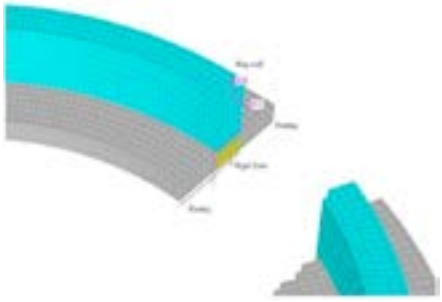

Figure 7: Foundation cross-section sample

All loading visualizations are illustrated with SAP2000. The internal forces of the shell elements are F11, F22, M11, M22, and V23, and these are indicated as limit values. These values have been selected for the reinforcements to be designed. Bending moment contours on footings, axial forces contours on footings, shear force contours on footings, ring wall bending moment contours, ring wall axial force contours (Circumference), ring wall axial force contours (Vertical direction), and ring wall shear force contours are analyzed with SAP2000.

Figure 8: Ring wall foundation design

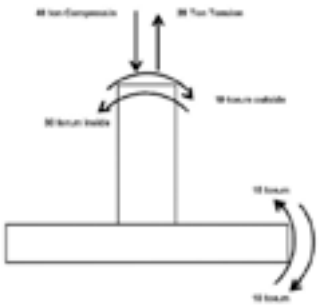

Figure 9: Minimum calculation of section for foundation

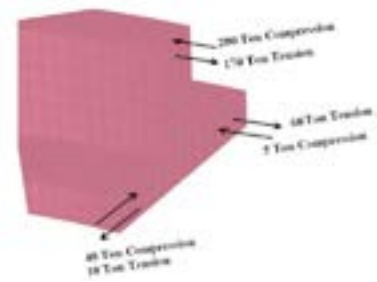

Figure 10: Axial force in circumferential direction

$$T_i = \frac{1}{\sqrt{2000}} \cdot \frac{C_i H}{\sqrt{\frac{t_s}{D}}} \cdot \frac{\sqrt{\rho}}{\sqrt{E}} \quad (1)$$

$$T_c = \frac{1.0404 \cdot \sqrt{D}}{\sqrt{\tanh\left(\frac{3.68H}{D}\right)}} \quad (2)$$

Equation 1 calculates the natural period of vibration for an impulsive mode of behavior and equation 2 calculates the natural period of convective (sloshing) mode of behavior [1].

Figure 11: M11 bending moment in footing (Top)

This reinforcement can carry about 248 kN.m of the moment. Therefore it can be used for all section having such a moment below this value.

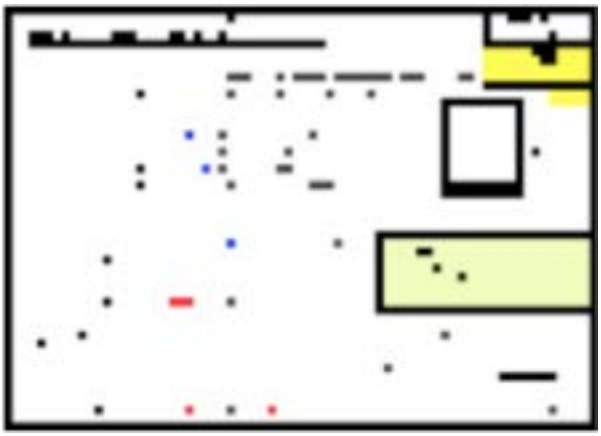

Figure 12: M22 bending moment in vertical direction

Equation 3 calculates the impulsive spectral acceleration parameter and equation 4 calculates the convective spectral acceleration parameter [2].

$$A_i = 2.5 \cdot Q \cdot F_a \cdot S_0 \left(\frac{I}{R_{wi}} \right) \tag{3}$$

$$A_c = 2.5 \cdot K \cdot Q \cdot F_a \cdot S_0 \left(\frac{T_S \cdot T_L}{T_c^2} \right) \left(\frac{I}{R_{wc}} \right) \tag{4}$$

Equation 5 calculates the effective impulsive weight of the product and equation 6 calculates the effective convective weight of product. Where Wp total weight of tank contents based on the design-specific gravity of the product [3].

$$W_i = \left(1 - \frac{0.218 \cdot D}{H} \right) \cdot W_p \tag{5}$$

$$W_c = 0.230 \cdot \frac{D \cdot W_p}{H} \cdot \tanh \left(\frac{3.67 \cdot H}{D} \right) \tag{6}$$

Equation 7 calculates the total design base shear. Where, Wf weight of the tank bottom, Ws total weight of tank shell and appurtenances, Wr total weight of fixed tank roof including framing, knuckles, any permanent attachments, and 10 % of the roof design snow load [4].

$$V = \sqrt{A_c^2 \cdot \left(W_s + W_r + W_f + W_i \right)^2 + A_i^2 \cdot W_c^2} \tag{7}$$

Equation 8 calculates the total combined hoop stress in the shell. Where, Nh product hydrostatic membrane force, Ni impulsive hoop membrane force in tank shell, Nc convective hoop membrane force in tank shell.

$$\sigma_T = \frac{N_h \pm \sqrt{N_i^2 + N_c^2 + \left(A_c \cdot N_h \right)^2}}{t} \tag{8}$$

Equation 9 calculates ring wall moment and equation 10 calculates slab moment [5].

$$M_{rw} = \sqrt{A_i^2 \cdot \left(W_i X_i + W_s X_s + W_r X_r \right)^2 + A_c^2 W_c^2 X_c^2} \tag{9}$$

$$M_s = \sqrt{\left(A_i^2 \cdot \left(W_i X_{is} + W_s X_s + W_r X_r \right)^2 + A_c^2 W_c^2 X_{cs}^2 \right)} \tag{10}$$

Course No.	Course width(m)	Y(m)	Course thk.(mm)	Course C.A.(mm)	σ_h (Mpa)	N_t (N/mm)	N_c (N/mm)	σ_s (Mpa)	σ_T (Mpa)	S_d (Mpa)	σ_{all} (Mpa)	Stress ratio	
1	2	16.5	10	3	138	121	1	12	150	137	182	0.83	OK
2	2	13.5	9	3	140	121	1	13	154	137	182	0.84	OK
3	2	11.5	8	3	143	121	2	15	158	137	182	0.87	OK
4	2	9.5	8	3	117	121	3	15	132	137	182	0.73	OK
5	2	7.5	7	3	115	116	6	16	131	137	182	0.72	OK
6	2	5.5	6	3	110	98	10	16	127	137	182	0.70	OK
7	2	3.5	6	3	68	71	17	12	80	137	182	0.44	OK
8	2	1.5	6	3	25	34	31	8	33	137	182	0.18	OK

Figure 13: Hoop stress

For 200 tons of tension in the circumferential direction along the ring wall, 200/3,650 = 55 cm^2 reinforcement should be 17.4 Ø 20. This means 18 Ø 20. Therefore, the reinforcements at the top of one meter of the ring wall should be 18 bars 1 meter high from the top. For simplicity, all 1.5 m ring wall reinforcements are used at the same value. The maximum tension in the vertical direction along the ring wall is about 30 tons, which requires 8.24 cm^2 of rebar. We have a value of 30 tons.m for the bending moment and the required rebar is 13.00 cm^2. So a total of 8.24 + 13.00 = 21.25 cm^2 and we can use Ø 20/20 for both sides [6].

3. CONCLUSIONS

In the method we use to model the structure, taking into account the ground and structure interaction, we first obtain the primary frequency of the structure. To do this, we enter the type of soil layers, the layer radius, soil shear modulus, poisson ratio, damping, and soil depth. This method gives us the movement and damping of the ground, which effectsthe structure.

It is clear that dynamic processes will occur in the soil environment during an earthquake in the study area. The shear wave propagating during the earthquake causes the groundwater pressure in the ground to rise and the amplitude of the shear strength to decrease. This reduction may cause some failures in the ground, depending on the amplitude of repetitive deformations. In addition, liquefaction develops depending on earthquake parameters such as the distance and magnitude of the earthquake source and the maximum horizontal ground acceleration in the study area.

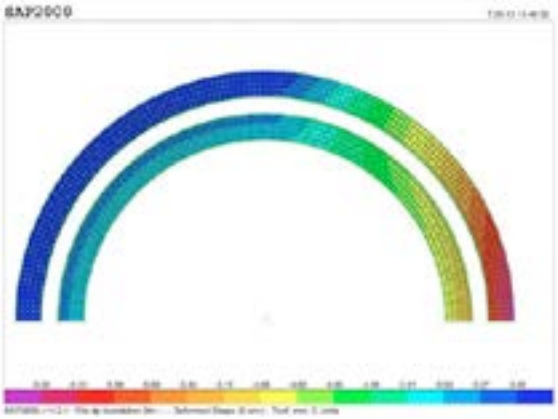

Figure 14: Soil deformation values

Considering these principles, evaluation methods that take into account all these factors have been proposed topredict whether there is a liquefaction problem or not. Accordingly, calculations were made based on the SD-13 drilling. The value of ah= 0.087 g was taken into consideration in the layers examined in relation to the ground movements that may occur in the study area due to the effect of dynamic loads that may cause liquefaction and an earthquake with a magnitude of M=7,5. The ground settlement calculation was made using the corrected SPT-N55 numbers obtained in the field.

$$\Delta H = \frac{31.2 \cdot q_{net}}{N} \tag{11}$$

The total settlement for foundations is calculated by the above equation. Where ΔH (cm) is the settlement that will occur in the soil layer, qnet (kg/cm2) is the structural load, N is the average SPT impact number and qnet will be taken as the amount of the total load of the structure corresponding to the unit area. The amount of the structure load corresponding to the unit area is accepted as 1.25 kg/cm2 and since the corrected average obtained in the field is SPT-N55 = 9, these values are substituted in the above equation and the total settlement ΔH = 4.33 cm is obtained. Since these obtained values are within the limit values, no settlement problem is expected on the ground. The results regarding stability control and anchor design are as follows. Since the maximum deformation is 6.5 mm and 37500 x 0.0065 = 243 kN/m2 < 405 = 270 x 1.5, there is no negative response, so the foundation can be considered safe. Tank anchor calculation is 5000 m3, seismic moment (N-m) Mrw = 76.821.330.27, tank and roof weight affecting the shell base Wt = 23400 N/m, Av = 0, D = 19 m. Per unit circumferential length the uplift load on the anchors is WAB and the anchor seismic design load is $P_{AB.}$

$$W_{AB} = \left(\frac{1,273 M_{OE}}{D^2} - W_t \left(1 - 0,4 A_v\right) \right) \quad (12)$$

$$P_{AB} = W_{AB} \left(\frac{\pi D}{n_A} \right) \quad (13)$$

Firstly, it is calculated as WAB = 248000 N/m from the related relations. Where, nA is to denote the number of equally spaced anchors around the tank circumference and PAB = 739784 N for nA = 20. An allowable tensile stress for anchor bolts and straps equal to 80% of the published minimum yield stress. With the analysis, it was found that the minimum yield stress of the bolts is 355 Mpa and the required area of a bolt is 739784 / (0.8 x 355) = 2605 mm^2. This gives a 57.8 mm diameter bolt.

In this study, a different solution method was proposed to transfer the seismic load to the foundation and to design the annular circumferential foundation, it was sufficient to induce the seismic shear force only in the center of gravity of the tank. This force was transferred to the ring wall by hypothetical rigid members. The computer software then multiplied the shear force by the loading distance to create the seismic moment. Therefore, there is no need to use both seismic moment and shear in the tank foundation model.

REFERENCES

[1] Bakalis, K., Seismic Performance Assessment of Industrial Facility Atmospheric Liquid Storage Tanks, 2018.

[2] Bektaş, N., Reliability Based Seismic Assessment of Unanchored Circular Steel Storage Tanks, 2020.

[3] Wisnugroho, J., Sutomo, Numerical Study of Oil Storage Tanks during Planar Settlement, 2018.

[4] Bakalis, K., Vamvatsikos, D., Fragiadakis, M., Seismic Fragility Assessment of Steel Liquid Storage Tanks, 2015.

[5] Keypour, H., İz, S., Tank Foundation Design, 2012.

[6] Welded Tanks for Oil Storage, API Standard 650 Thirteenth Edition, 2020.

Research Article

USING DEEP LEARNING ON SYSTEM IDENTIFICATION OF THE RETAINING WALLMODEL

SERTAÇ TUHTA[1]

[1]*Department of Civil Engineering, Ondokuz Mayis University, Samsun, Turkey, stuhta@omu.edu.tr, ORCID: 0000-0003-2671-6894*

ABSTRACT

Structures have been adversely affected by dynamic effects from past to present. This has alwaysbeen a problem for structural engineering. Structural engineers strive to design structures to be least affected by dynamic effects. The biggest challenge in these designs is the exact and realistic calculation of the response of dynamic effects on the structure. There are various methods for calculating the dynamic effects affecting the structures. The system identification method is one of the methods used to calculate the responses of the structures to the dynamic effects affecting. In the other words, a Mathematical model of the structure system is obtained by the system identification method. Today, the use of artificial intelligence has increased considerably in every field. In the field of system identification, methods using artificial intelligence (neural network) have been used in many studies in training data. For this reason, in this study, the system identification of the retaining wall model was made with the deep learning method. In the light of the data obtained, it was seen that the system identification of the model was realized close to one hundred percent. As a result of this study, it is seen that deep learning will be useful on system identification methods in the civil engineering field.

Keywords: *System Identification, Deep Learning, Artificial Intelligence, Neural Network, Retaining Wall.*

1.INTRODUCTION

Today, studies and developments about earthquake resistance of structures are

Received: 23.04.2022 - Accepted: 12.07.2022
DOI: 10.17932/EJEAS.2021.024/ejeas_v02i2002

very popular. There are many old and new methods used especially when determining the earthquake performance of structures. The methods used in the past century and the beginning of the 21st century have been replaced by newer and more reliable methods. The old methods are *generally theoretical and based on* some assumptions. The new methods, on the other hand, include more experimental methods and the data represent more real situations. The system identification method is one of these methods. System identification (SI) is a modeling process for an unknown system based on a set of input outputs and is used in various engineering fields [1], [2]. With system identification, a mathematical model of the system is created. Effects and reactions on the created model are determined realistically by the mathematical model. In determining the earthquake performance, it is of great importance to obtain the mathematical model of the structure or model correctly. It is known that it is possible to obtain correct earthquake performance only with the correct mathematical model.

The system identification method also includes various improvements. Especially today, the use of artificial intelligence is seen in many areas. In the field of system identification, its use in obtaining parameters and processing data is seen in current academic studies. The authors have many studies [3-19] on system identification and artificial neural network given in the sources. It has been clearly seen that the limits of deep learning are pushed by covering various models in these academic studies. Based on all this information, the very up-to-date deep learning method was used on system identification in this study. It was decided to choose the retaining wall model as the model. Also, it is aimed to interpret the data obtained in the study by sharing it clearly in the results section.

2.DEEP LEARNING

Deep learning is part of a broader family of machine learning methods based on artificial neural networks with representation learning. Artificial neural networks as defined above are implemented in computer software as learning systems that match inputs to outputs. They are designed to perform the mathematical operation of "simultaneously organizing low-level visual information in a hierarchical structure and then mapping the resulting structure back into the input," in contrast to, say, a traditional vector or matroid, in which the input would be treated linearly or an idealized monoid where the model has an associative structure. Deep learning itself often requires some form of pre-training, a period of trial-and-error based on artificial neural network models where training data are fed into the model through layers of progressively more complex activation functions. This involves defining rules about how to generate neural network representations for particular data, then generating thousands or even millions of models for a data set. A network, which might contain millions of connected

neural layers, is trained by comparing its predicted outputs with the actual outputs of the network. The model is trained by feeding it with more and more examples, progressively reducing its accuracy until the output matches the input. The accuracy, or the ability of the network to correctly classify a data item, increases with the size of the input set and with a decreasing number of layers in the network. The ability of the network to adapt to new examples can be measured by the number of times it is classified on average when the data are compared with new examples.

For example, a network with three layers that can accurately classify an input with two features could perform better than a network with a single layer that would only successfully classify the input with three features. The best networks perform so well that, as the number of training examples increases, the network becomes "smooth". For example, a network that can classify a new image with only four examples will show a nearly perfect function until the network is labeled with 64 examples. This is called "lateral inhibition". The number of samples usually used to achieve this is referred to as the "generative model size". Note that if the output of the network matches the actual input a model with a larger number of layers is considered to be a more robust representation of the real data, and can be used to classify it on the fly, without the need to redo all the work in a previous layer. Deep learning is a subset of machine learning. It usually describes the connection between an input signal (the input layer), a hidden layer (the hidden layer or the hidden- mean layer), and an output signal (the output layer or the output layer). However, other machine learning techniques work similarly. For example, finite element models can generate complex systems by considering several different possible solution parameters and then feeding the output from one of these parameters into another, with subsequent evaluations until a solution is found. In contrast, a deep model starts with some hidden state and then works backward through time to find a possible solution. This is the first major concept in deep learning: identifying the output signal and making it the input. If this input is a pre-trained model, we can return to the neural network and select the output that best matches the input. For example, consider a network trained to discriminate between an image of a cat and an image of a dog. Let the hidden layer be the set of multi-layer artificial neurons, each with two outputs and one hidden input. If we want to make this network match the image of the dog and instead match the cat, we need to find the hidden states that best match the input. To do so, we would first consider how a prior distribution will divide the set of hidden states into those that match the input (i.e., the X set) and those that don't (the Y set). Then we will look for the hidden states that match the Y set. When this set is found, the hidden state of the output neuron of the corresponding hidden layer is chosen. Deep learning is related to Bayesian

networks and multilayer perceptrons (MLPs). Bayesian networks are based on the assumption that they are discrete systems with states (points in space or time), which can be observed at each time step. It also assumes that there is only one hidden layer. A perceptron is a basic deep learning algorithm with one hidden layer, also known as a feed-forward neural network. These learning networks are capable of combining multiple inputs into one output. This is sometimes called "many hidden layers". They are based on the assumption that the hidden layers of the network are useful only for training the hidden layer, which returns a "predictable output". The main distinction between deep learning and these previous approaches is the possibility to apply back-propagation, which works at the hidden layers, by dividing the training set into a set of pattern matrices, each consisting of a set of N features. And an associated error vector and iteratively reducing the error by using the input vectors as input. Since the hidden layer is responsible for classification, a classifier trained with this system cannot be used directly as input to other neural networks. Multi-layer perceptrons are based on the hope that the hidden layers would serve a useful purpose. For instance, the deep belief network can be adapted to the perception of natural scenes. Finally, there is the not-yet popular neural network architecture. This has gained momentum in recent years due to the advent of large amounts of computing power and the availability of new research papers. This architecture consists of multiple neurons in each layer that all produce outputs that add up to make one output. The outputs from each neuron in the layer are fed into the neurons below, producing a "super-dense" neural network. This way, the input signals are not isolated by distance in the network.

Currently, deep learning is already changing the world in many ways. Take self-driving cars, for example. Many automakers are currently racing to develop a car that can drive itself without a human driver. This may sound like science fiction, but recent breakthroughs in deep learning have enabled these cars to drive on the highway autonomously. As a result, when an accident happens, a car that has no driver will be more likely to avoid the crash than one driven by a human. These are still early days, and not all companies in the self-driving car industry are sharing the importance of deep learning in their technologies. There are several challenges that businesses need to consider as they adopt new technologies. Below are some of the business implications. Deep learning algorithms provide a quantitative measure of the quality of the algorithms and their performance in different scenarios. Hence, as a business, you will need to measure the success or failure of your deep learning algorithm. To do so, you need to have a detailed understanding of the problem that you want to solve, what kind of problem you are trying to solve, and how deep learning can help you address the problem. For instance, if you are trying to solve a fraud detection problem, you should look

for a deep learning algorithm that is capable of distinguishing between different types of fraudulent transactions. A good fraud detection solution should be able to differentiate between intentional transactions and those that are unintentional. In the second instance, if you are trying to build a chatbot, you should look for a deep learning algorithm that is capable of understanding human commands and responses. Finally, you can start learning the mathematical concepts of deep learning. In order to accurately develop a deep learning algorithm that is capable of solving the specific problem you are trying to solve; you need to develop an understanding of the underlying mathematics. When it comes to the business value of deep learning, there are two broad questions that are essential to answer. The first is "how deep learning makes the business data cleaner?" In most cases, the answer to this question is "very". The second question is "what business problems do deep learning solutions for businesses?". In order to answer this question, you need to define the value of the business problem to the business. In the early days of deep learning, most of the initial focus was on applying deep learning to better picture objects in videos or images. However, deep learning is much more versatile than this and can be applied to a variety of business problems. As a result, many companies are now adopting deep learning to solve business problems in different industries. In general, there are three types of deep learning algorithms. Each of these algorithms comes with a specific set of advantages and disadvantages, and a lot depends on your specific business problem. To understand the benefits and disadvantages of the various algorithms, you need to know the algorithms' source code. Fortunately, there are some excellent deep learning source code blogs that explain how to read the source code of different deep learning algorithms in detail, and how to perform most basic research in this field. So, let's jump into deep learning. Deep learning can be used in almost any industry. It has been used in fields such as cyber security, genomics, robotics, speech recognition, search engines, and autonomous cars.

The difference between machine learning and deep learning are given in Figure 1.

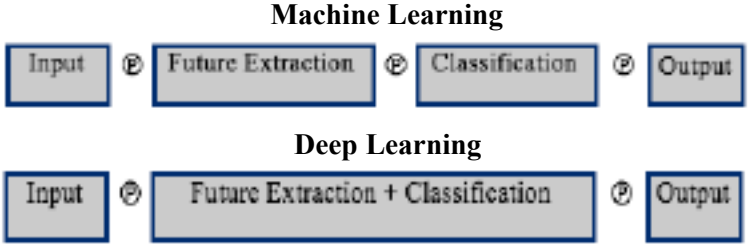

Figure 1. Difference between machine learning and deep learning

3.DEEP LEARNING METHODOLOGIES

Algorithms in the first generation of machine learning are known as back-propagation algorithms, an idea from the 1940s. Back-propagation involves linear and unidirectional control and estimates the weights and biases that need to be corrected for the target output variable. The aim is to generate an output value from an input value to determine the errors in the prediction model. Back-propagation algorithms were developed in the late 1960s by Stanley J. Koopman and Konrad Zusek, and further developed by several other groups. The first example of backpropagation algorithms can be found in the unpublished article "Learning with error and noise" by John H. Conway and Walter Pitts published in 1973. Other early and notable work in the first generation of machine learning algorithms includes work on kernel learning, neural networks, and linear classifiers. A deeper understanding of these algorithms was helped by work done by Koopman and Zusek and by Donald Michie. Michie and Koopman published a seminal paper on back-propagation, using it to learn the relations between a binary classifier and its response variable. Back-propagation is a linear classifier. For example, if there are two possible choices for input, then the input and the output can be encoded in a single vector. This works well for binary classifiers, such as the binary classifier used to calculate credit scores. In binary classification, the output can be interpreted as a variable, such as whether a person is a male or female. But this can be complicated for more complicated classes, such as most legal indicators, where any variable might hold different information. Back-propagation algorithms learned by using this approach were able to learn this classifier.

4.NEXT-GENERATION MACHINE LEARNING ALGORITHMS

These are the seven main types of deep learning algorithms. Each of these algorithms has its strengths and weaknesses, so it is important to understand which type of algorithm you should use in a given case before you make your decision.

Neural Network: Neural networks are programmed to carry out specific tasks that have been defined by an algorithm. The different tasks that neural networks can carry out include classification and labeling, clustering, and deep learning. They are of great help in the areas of computer vision, image processing, speech recognition, and natural language processing.

Neural Network Paradigms: In this type of algorithm, the problem to be solved is described by a pattern (data structure). Then, the neural network is trained to use only this pattern to solve the problem. However, in deep learning, this means that the pattern must be uninterpreted and not intuitive. Examples of such uninterpreted patterns include having several units (cells) in a tree or having an

input on which the hidden units have to find the pattern. However, these uninterpreted patterns are often more challenging to implement in the neural network. However, while the algorithm requires having a vision and a pattern at the same time, this is a basic and necessary component to be able to deal with such problems. The most common types of algorithms that can be used for this are support vector machines, deep clustering, support vector machines with anti-correlations, and ridge regression.

Hierarchical Decisions Engine: It is an algorithm that considers the differences between two points to decide which one is larger or smaller. One of the methods of implementation of this algorithm is called the transfer function. In this type of algorithm, the decision maker first identifies two points in space and then tries to decide which one is larger or smaller. Some values are 0 and some values are 1, with 1 being the smallest and 0 being the largest. The algorithm first determines the smallest value, and then the larger of the two values.

Sparse Data Network: In this algorithm, only a small part of the information in a data set is considered. It can help when data is sparse and sparse data is difficult to process or manipulate. This method is different from classical data compression techniques, which have a fundamental limitation on the compression ratio. With minimal information on the data set, each additional element will have a lower compression ratio.

Hyper-parameter Machine Learning: Hyper-parameter machine learning is an optimization technique that allows users to select the parameters that have the greatest impact on the output of a neural network. It involves carefully choosing the values of the parameters and applying them to the data. Several different machine learning techniques are designed to help users decide which parameters to use and how much tooptimize them, and several hyper-parameter machine learning algorithms have been developed. HML is designed to solve regression and classification problems in as few steps as possible. There are many different types of hyper-parameter machine learning algorithms, but we'll focus on hyper-parameter classification algorithms and algorithmically based HML.

Supervised: This is an algorithm that can be used to take random data and classify it into categories. For example, it can classify structures into the two categories of "safe" and "not safe". It helps in reducing the errors that usually occur in order to classify and identifies whether two objects belong to the same category. There are several classification algorithms for image classification that have been developed by researchers worldwide. The popular ones are SVM, Naive Bayes, and Support Vector Machine (SVM).

Unsupervised: Unsupervised learning algorithms can be used to identify objects and classify them into different groups or classes. It helps in dealing with instances in which there is no clear classification in the data. The algorithm also helps in identifying a relationship between two objects. For example, the algorithm can be used to understand if two paintings belong to the same style or belong to different styles. Unsupervised learning algorithms also help in providing personalization in order to personalize results in the business process. It can also be used to identify objects in which the database is missing information. This can be used to provide information to consumers or employees. It also helps in visualizing the data on a given topic to identify any weak correlations between different variables.

5.APPLICATIONS IN CIVIL ENGINEERING

Some problems can be solved directly in optimization, but not using a stochastic gradient descent method. These include many kinds of constraint satisfaction problems. Another example is limited set problems, where the set of solutions to the problem must be small and the solution to be defined to be a subset of the solution set. These problems are well suited for dynamic programming algorithms. The basic idea is to update a set-selector function at regular time intervals (sources), instead of iteratively computing a stochastic gradient descent. A newer method for constrained set problems is to assign each element of the problem as a constraint set that can be searched for solutions. The relative dependence of subcomponents of a solution, but not in the general solution, is often useful in reinforcement learning. Often, the best learning can be obtained by simulating a large number of learning iterations, so the learning may be influenced by prior knowledge about the most probable solutions. However, solving a general optimization problem directly may be computationally expensive. Instead, the trained network can try to optimize the solution set in each iteration. For example, in linear programming, the optimal solution consists of a solution to the linear part of the problem, plus a sub-linear solution (a solution involving fewer unknowns than the linear part), with a small error term given by the gradient of the objective function. So, the sub-linear solution may be the solution to the linear part of the problem, with a small error term given by the gradient of the objective function.

The optimization problem may be solved in a sequence of iterative sub-optimizations. The sub-optimal values, chosen so that the cost decreases quadratically with the number of iterations, are called intermediate solutions. The use of sub-optimization has been considered efficient by applying approximation techniques. A smaller number of iterationsmay lead to better results. This technique can be easily combined with neural networks. Neural network optimization can

be described as a method to find a sub-optimal solution from the optimal solution. Using a neural network to find an approximate solution to a single (rather than a compound) optimization problem may have several advantages. The advantage is that the sub-optimal solution could be optimal in the sense that it approximates an approximate solution, but the network can achieve an error estimation better than random estimation, which would be impossible with random estimation. Another advantage is that the sub-optimizations are small, which makes them easy to estimate. Therefore, the sub-optimizations can be focused on sub-problems and reach the desired minimums, but not the maximums. The sub-optimizations may be chosen by fitting an effective optimizer that controls the choice of sub-optimizations. The cost function is evaluated on the suboptimal solution and all the sub-optimal solutions simultaneously. In other words, in the single-kernel formulation, the cost is only evaluated on the optimal solution (the stationary point) and all the suboptimal solutions simultaneously. Furthermore, the sub-optimal solutions may be used for the learning process itself. Finally, the sub-optimizations can be combined with the sub-optimal optimizers, allowing the sub-optimal solution to be used for the learning process itself.

Deep learning involves deep neural networks, which are essentially large-scale artificial neural networks that are trained by an algorithm. This algorithm requires massive amounts of data to be fed into the algorithm, which is referred to as training data. The data must be clean and characterized in order to produce good results. Here, deep learning can be applied to solve the following two related problems:

Environmental planning: The problem of predicting the outcome of building structures on site has been difficult for many engineers due to the complexity and ambiguity of the process. Deep learning helps engineers to discover the best way to build their structures on-site without having to worry about the complicated process of designing the construction of the structure itself. This is because the engineer can first figure out which structural materials to use and the main constraints to the design. The result is a simpler, more robust, and more cost-effective project.

Building management: Real estate firms have been challenged to use technology to manage and handle their data. This type of data is large and complex, and there are large volumes of information to be managed. Deep learning has become an important tool in the field of real estate management and especially in the form of cloud software. This technology has the potential to revolutionize property management. It can process millions of data points in real-time and identify patterns and trends that make it easier to predict the behavior of property value over time. Another example of data that is hard to deal with and has been difficult

for engineers to predict is oil and gas production. This has led to the widespread adoption of computational fluid dynamics for oil and gas production. Finally, deep learning can also be used for large-scale modeling. It has the potential to reduce modeling costs by up to 20% for engineers. Deep learning is making a profound impact on the way engineers perform their work. It has provided a new set of tools for analyzing, modeling, and predicting. It also has the potential to revolutionize the way people and companies build things and also use data.

6.DESCRIPTION OF RETAINING WALL MODEL

Retaining walls use is very popular. It attracts attention with its practicality and simple geometry. Their production is also very practical. The retaining wall model is designed entirely of concrete. The concrete used is C30-TS500. The retaining wall model was chosen to choose a simpler model instead of complex building systems. In addition, the geometric structure of the model was also effective in this choice. The cross-section of the retaining wall is L-shaped. The length of the retaining wall model is 6 meters. The height of the retaining wall model is 3 meters. The base width of the retaining wall model is 3 meters. The thickness of the upper wall and the lower table is 0.25 meters. The dimensions of the retaining wall model are also given in Figure 2. The three-dimensional view of the retaining wall model is given in Figure 3.

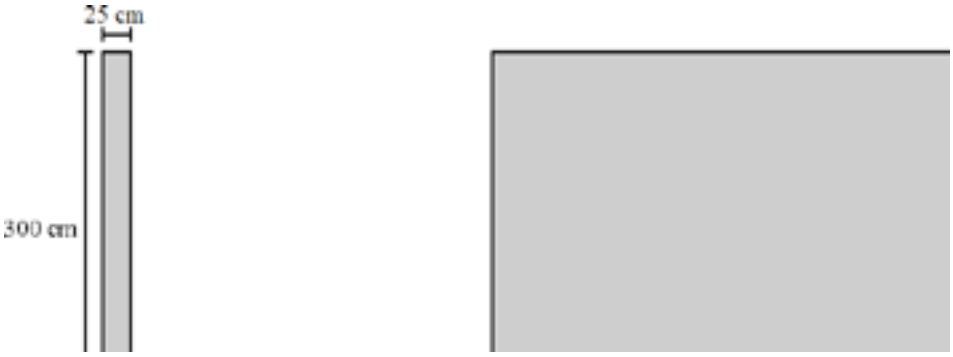

Figure 2. The dimensions of the retaining wall model.

Figure 3. 3D view of the retaining wall model

7.RESULTS AND DISCUSSION

MATLAB 2018b software program deep learning toolbox was used to obtain all the results. Obtained results are shared as figures. Figure 4 shows the training progress of the neural network.

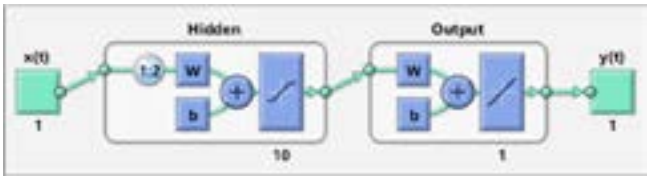

Figure 4. Neural network process

The input used in the study are given in Figure 5.

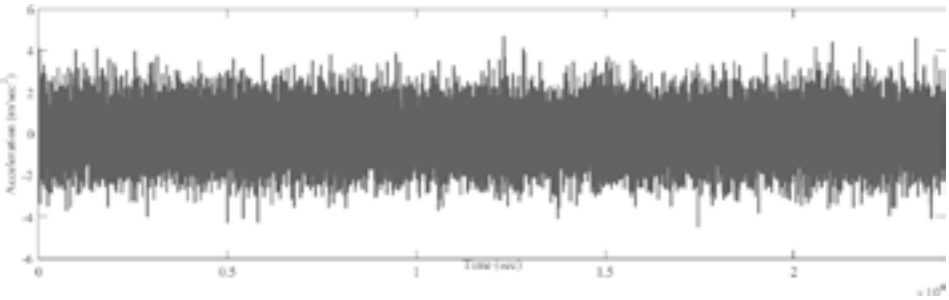

Figure 5. Input

The output used in the study are given in Figure 6

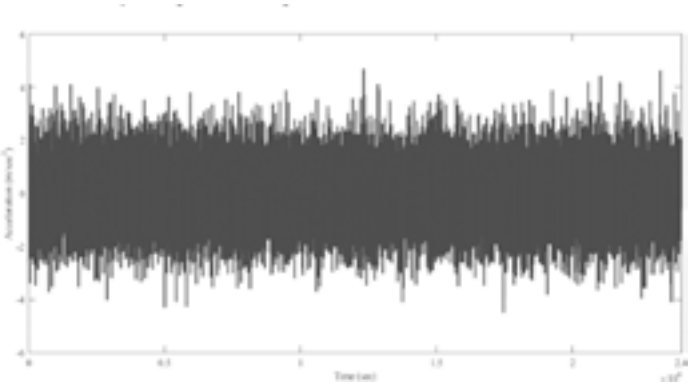

Figure 6. Output

The retaining wall model's frequency obtained is given in Figure 7.

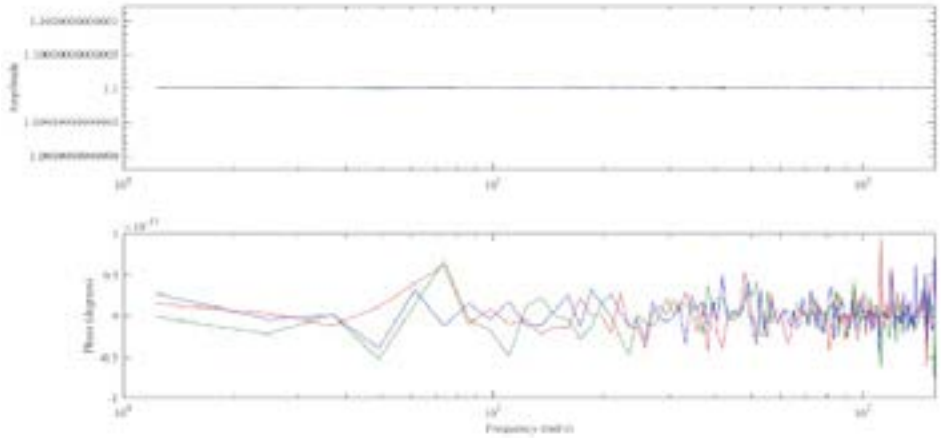

Figure 7. Frequency

The retaining wall model's periodogram obtained is given in Figure 8.

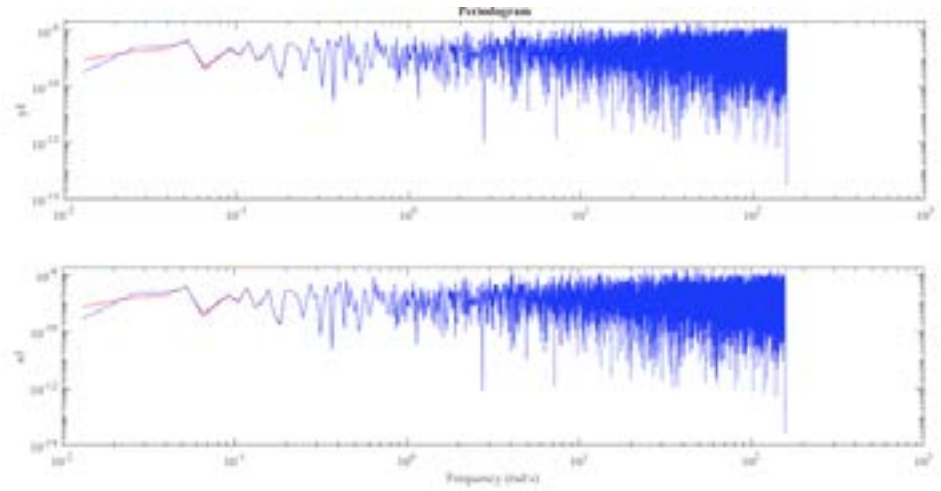

Figure 8. Periodogram

The retaining wall model's poles and zeros obtained is given in Figure 9.

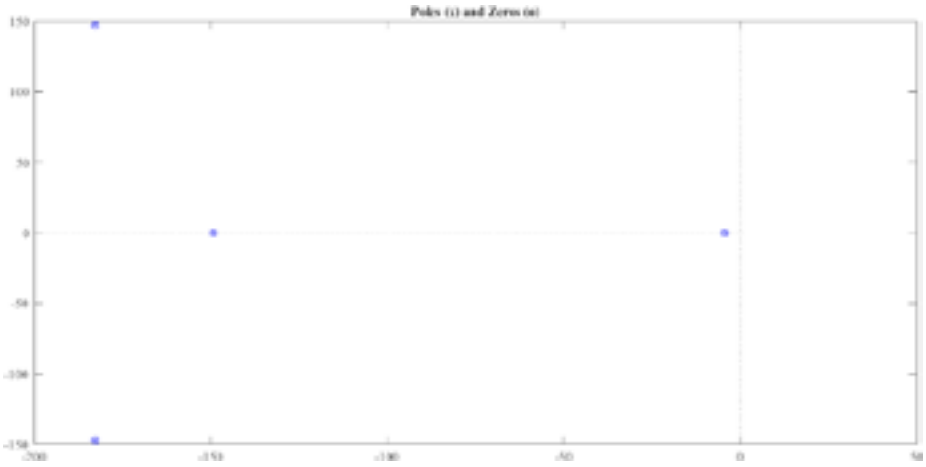

Figure 9. Poles and zeros

The retaining wall model's residuals obtained is given in Figure 10.

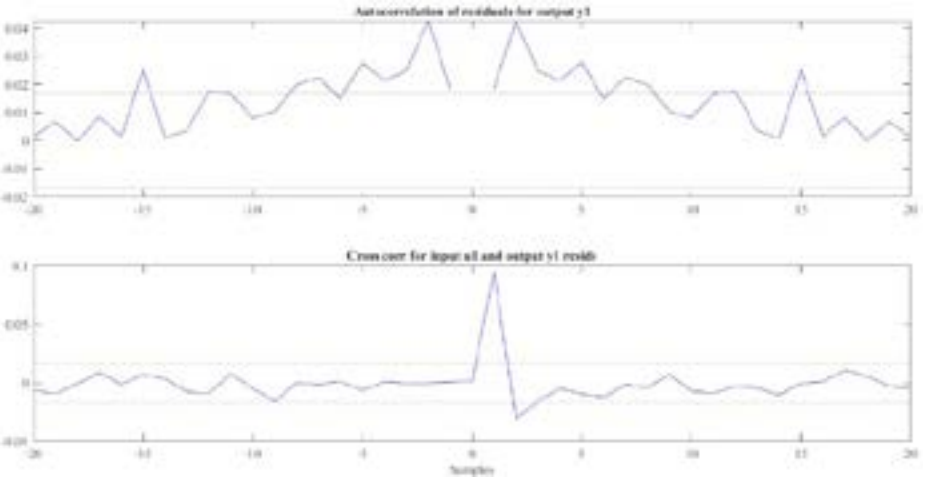

Figure 10. Residuals

The retaining wall model's error histogram obtained is given in Figure 11.

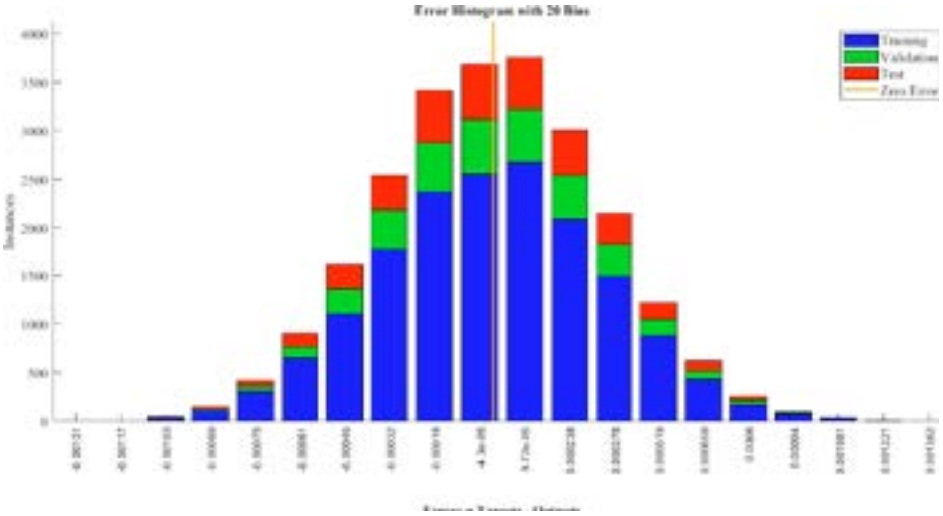

Figure 11. Error histogram

The retaining wall model's response of output element obtained is given in Figure 12.

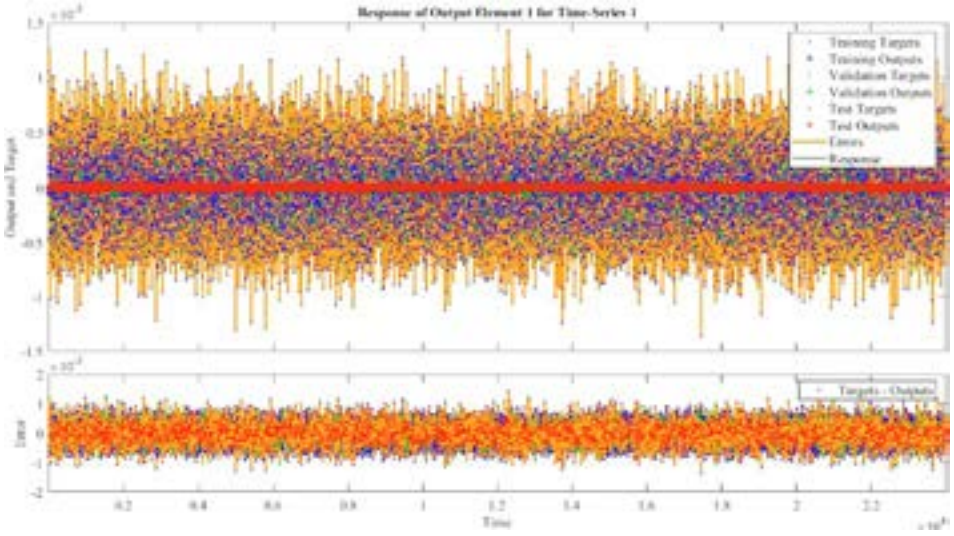

Figure 12. Response of output element

8.CONCLUSION

As a result of this study, the following graphics belonging to the retaining wall model were obtained.

- The retaining wall model's frequency
- The retaining wall model's periodogram
- The retaining wall model's poles and zeros
- The retaining wall model's residuals
- The retaining wall model's error histogram
- And the most important; The retaining wall model's response of output

When all the findings are examined, it is seen that the deep learning method makes very successful predictions on system identification. Thus, it is predicted that the accuracy and reliability of the data to be used in the future will increase. In addition, the processing speed and practicality of the deep learning method attracted a lot of attention. In the light of all this information, the deep learning application on an L-shaped retaining wall model was tested in terms of accuracy, practicality and utility, and successful results were clearly obtained. It is thought to be particularly successful in early warning systems against dynamic loads. In addition, it is recommended in the field of data processing and evaluation in civil engineering on the other words system identification.

REFERENCES

[1] G.F. Sirca Jr., H. Adeli, System identification in structural engineering, Scientia Iranica A (2012) 19 (6), 1355-1364

[2] J. Kim, System Identification of Civil Engineering Structures through Wireless Structural Monitoring and Subspace System Identification Methods, PhD thesis, University of Michigan, 2011.

[3] S. Tuhta and F. Günday, "MIMO System Identification of Industrial Building Using N4SID With Ambient Vibration," International Journal of Innovatıons in Engineering Research and Technology, vol. 6, no. 8, pp. 1–6, Aug. 2019.

[4] S. Tuhta, F. Günday, H. Aydin, and M. Alalou, "MIMO System Identification of Machine Foundation Using N4SID," International Journal of Interdisciplinary Innovative Research Development, vol. 4, no. 1, pp. 27– 36, Jul. 2019.

[5] S. Tuhta, F. Günday, and H. Aydin, "Subspace Identification Using N4SID Methods Applied to Model Concrete Chimney," JournalNX, vol. 6, no. 6, pp. 415–423, Jun. 2020.

[6] S. Tuhta and F. Günday, "Multi Input - Multi Output System Identification of Concrete Pavement Using N4SID," International Journal of Interdisciplinary Innovative Research Development, vol. 4, no. 1, pp. 41– 47, Jul. 2019

[7] S. Tuhta and F. Günday, "System Identification of RC Building Using N4SID," International Journal of Research and Scientific Innovation, vol. 6, no. 11, pp. 100–106, Nov. 2019.

[8] S. Tuhta, F. Günday, and M. Alalou, "Determination of System Parameters on Model Lighting Pole Using ANN by Ambient Vibration," International Journal of Research and Scientific Innovation, vol. 6, no. 11, pp. 191–195, Nov. 2019.

[9] S. Tuhta, I. Alameri, and F. Günday, "Numerical Algorithms N4SID For System Identification of Buildings," International Journal of Advanced Research in Engineering Technology Science, vol. 6, no. 1, pp. 7–15, Jan. 2019.

[10] S. Tuhta and F. Günday, "Modal Parameters Determination of Steel Benchmark Warehouse by System Identification Using ANN," International Journal of Research and Innovation in Applied Science, vol. 6, no. 12, pp. 8–12, Dec. 2019.

[11] S. Tuhta and F. Günday, "Artificial Neural Network Based System Identification Usage for Steel Sheds," International Journal of Innovations in Engineering Research and Technology, vol. 7, no. 10, pp. 22–30, Oct. 2020.

[12] S. Tuhta and F. Günday, "Dynamic Parameters Determination of Concrete Terrace Wall with System Identification Using ANN," JournalNX, vol. 6, no. 9, pp. 195–202, Sep. 2020.

[13] S. Tuhta and F. Günday, "Study for Artificial Neural Network of Aluminum Benchmark Bridge," International Journal of Research and Innovation in Applied Science, vol. 5, no. 2, pp. 90–95, Feb. 2020.

[14] S. Tuhta, F. Günday, and H. Aydin, "Nonlinear System Identification of Model Concrete Chimney Using Hammerstein Wiener Models," presented at the Global Congress of Contemporary Study a Multidisciplinary International Scientific Conference, 2020.

[15] S. Tuhta, F. Günday, and H. Aydin, "Example for Nonlinear System Identification of Model Masonry Retaining Wall with Hammerstein Wiener Models," presented at the A Multidisciplinary International Scientific Conference on Science, Technology, Education and Humanities, 2020.

[16] S. Tuhta, F. Günday, and H. Aydin, "Nonlinear System Identification of Model Concrete Chimney Using Hammerstein Wiener Models," presented at the Global Congress of Contemporary Study a Multidisciplinary International Scientific Conference, 2020.

[17] S. Tuhta, F. Günday, and H. Aydin, "System Identification of Model Steel Bridge with Genetic Algorithms," International Journal of Research and Innovation in Applied Science, vol. 5, no. 1, pp. 55–59, Jan. 2020.

[18] S. Tuhta, F. Günday, and H. Aydin, "System Identification of Model Steel Bridge with Fuzzy Logic," International Journal of Research and Innovation in Applied Science, vol. 5, no. 1, pp. 50–54, Jan. 2020.

[19] S. Tuhta, F. Günday, and A. Alihassan, "System Identification of Model Steel Chimney with Fuzzy Logic," International Journal of Research and Innovation in Applied Science, vol. 5, no. 1, pp. 11–15, 2020.

[20] MATLAB and Statistics Toolbox Release 2018b, the Math Works, Inc., Natick, Massachusetts, United States.

Research Article

COVID-19 FAQS CHATBOT USING ARTIFICIAL NEURAL NETWORK WITH BAG OF WORDS

ABDELRAHMAN R. S. ALMASSRI*[1]
NOUR AMMAR[1], UFUK FATİH KÜÇÜKALI[2]

[1] Department of Software Engineering, Istanbul Aydin University, Istanbul, Turkey
[2] Department of Architecture, Istanbul Aydin University, Istanbul, Turkey
**E-mail address: abdelrahmanalmassri@stu.aydin.edu.tr, noor101ammar@gmail.com,ufkucukali@aydin.edu.tr*
ORCID: 0000-0001-5450-7956, 0000-0002-2691-4180, 0000- 0002-2715-7046

ABSTRACT

COVID-19 is a contemporary virus with a fatal syndrome that had not been seen in the last century. The virus evolves in people of all ages in all areas around the world. As the increment of cases is growing up rapidly the worry of people is increasing, which makes it very hard for healthcare departments and governments to solve people's queries. AI solution is suggested, where a simulation of front-desk assistance. Chatbots are easy to use and simulate a human conversation through text via smartphones or personal computers. Chatbot applications can improve patient information, monitoring, or treatment adherence. The architecture is a simple neural network consisting of a single hidden layer and the sigmoid function is trained by textual data organized by multiple data organization methods. A simple GUI is provided to the classifier to be tested practically. Data used is a collection of questions and their answers about COVID-19. The approach has achieved acceptable results considering speed, and accuracy. Practical predictions were true with acceptable accuracy.

Keywords: *FAQ's, Healthcare, COVID-19, Chatbot, Neural Network, NLP.*

Received: 26.05.2022 - Accepted: 17.07.2022
DOI: 10.17932/EJEAS.2021.024/ejeas_v02i2003

1.INTRODUCTION

In the last two years, a new disease had been discovered on 31 December 2019 named COVID-19 virus. It has involved the whole world and is considered to be announced by WHO as an official pandemic on 11 March 2020, which spread anxiety between nations. Hence, people want to query about the new virus, its symptoms, and its fatality, which creates an issue of shortness in front-desk assistance employees as well as health call centers employees. To deliver the information to a bigger number of people, an Artificial Intelligence solution is suggested. A chatbot is an automated software program that interacts with humans. A chatbot is an automated computer program that fundamentally simulates human conversations such as the works of [1, 2, 3]. The evaluation of the chatbot's User Interface (UI) that was done for COVID-19 in [4] shows that the best approach is the interactive chatbot that can answer the user in conversational way and accept the free hand input, which depends on AI as this paper introduces. There is different architecture to classify text, and the word2vec embedding model [5] and GloVe [6] are embedding dictionaries, while a bag of the word (BoW) [7] and BoW TF-IDF [8] are vectorization methods that convert the textual data to numeric data in vectors shape. The artificial Neural Network (ANN) used consists of one hidden layer that uses sigmoid function and synaptic weights. The result of the architecture was fair enough to accept since the data is complex and unlike [8, 10, 11] where they used classification depending on multiple classes, in our approach, there is one class to predict which is the true question itself. The approach predicts the user's input question to its most similar true question in the dataset, then prints its answer in the Graphic User Interface (GUI) chatbot. The experiment compared with three models BERT, TF-IDF, and GloVe in section 5.

2.THEORY

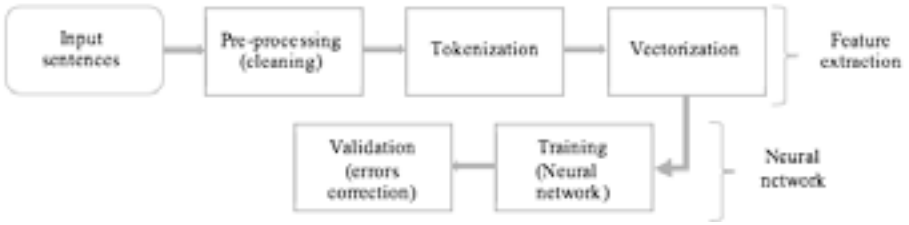

Figure 1. the algorithm flowchart of our approach

Text vectorization method used is Bag of Word [7]. The occurrence calculation used is the binary occurrences where 1 refers to the existence of a word and 0 refers to non-existence in the whole dataset, which makes it a dictionary consisting of 1688 vectors referring to several tokens, as shown in Table 1. Bert model [11], TF-IDF Representation [8], and glove embedding dictionary [6] are other models used to organize textual data. In this paper, they are applied for comparison.

Table 1. simulation of Bag of Words vectorization process applied on dataset

		Word and its series							
		1	2	3	4	5	6	…	1688
Sentence and its series		"have"	"question"	"corona"	"disease"	"headache"	"…"	"symptom"	
	"I"								
1	"I have a question about corona … symptoms"	1	1	1	1	0	0	…	1
2	"is headache beinga symptom of corona disease?"	0	0	0	1	1	1	…	1
…	…	…	…	…	…	…	…	…	…
642	"what is corona?"	0	0	0	1	0	0	…	0

BoW most used method in text classification method because of its simple approach to solving classification problems [10]. BoW representation takes the sentence $x_i = \{x_1, x_2, x_3\}$ and converts it to a vector of ones and zeros $v_i = \{x_1, x_2, x_3\}$ then includes it into a matrix $v_i = \{v_1, v_2, v_3\}$.
NLTK (Natural Language Tool Kit) is a high functional NLP platform from TensorFlow that process textual data. This project is used in phases 1 and 2. Methods used are: stem() to stem the text, lower() to apply lower case, and word tokenize() to apply the tokenization process.

First phase as shown in Figure 1 is preprocessing the data by cleaning it of any punctuation marks such as (?,!,'," ", .,,), after the cleaning stemming process is applied to data then apply lower case on the whole text. Stemming is defined as reducing inflection in words to their root forms such as (saw → see, looks → look, sking → ask) to reduce the number of words that enter the tokenization process. The second phase is tokenizing the clean data which means taking the meaningful words and meaningless words such as (a, the, at). The third phase is vectorization after Features are selected in phase 2, the tokens in each sentence are numeric values in vectors as simulated in figure (BoW).

The model consists of one hidden layer multiplied by the sigmoid function, as well as input and output layers with a total of 3 layers. 30 hidden neurons in the hidden layer and 0.01 learning rate ratio (Figure 2).

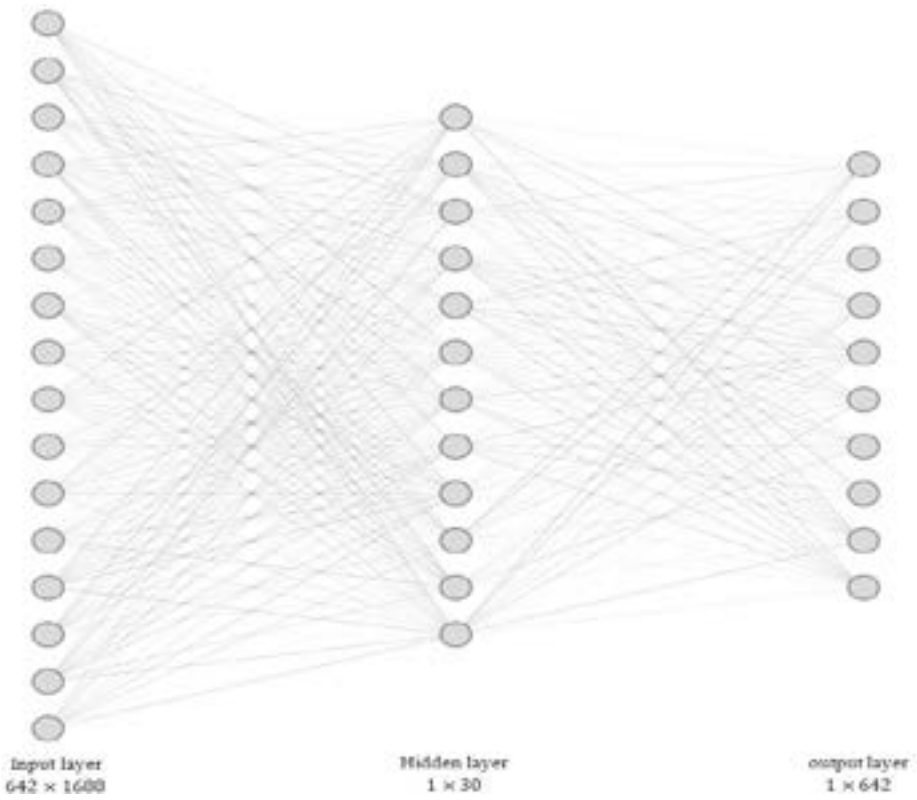

Figure 2. Simulation of ANN of our approach

Synaptic weight Refers to the measure of amplitude-change in a single iteration of the learning batch-of connection between nodes [14]. Where y_i is the output of one layer, w_i refers to weights and x_i refers to the binary BoW vectors.

$$y_i = \sum_i w_i x_i$$

Backpropagation [15] is used in this approach to learn Gradient decent, a is the learning rate which $a = 0.01$,where Δw_i refers to weights (y_i-y_i) is the evaluation of error as specified in (4).

$$\Delta w_i = (y_i - y_i)_i$$

Layers as simulated in Figure 2. The input layer is the bag of words sequences number of dimensions is 642 × 1688, where 642 refers to the number of sentences and 1688 refers to the length of BoWs sequences (each sentence converted to a numeric vector). It is multiplied by the sigmoid function (3).

The sigmoid function that first suggested by [15] and approved its functionality in backpropagation learning networks. In our method, it is used to normalize values since it is the most useful activation function for the textual prediction that applies feature selection on one probability between 0 and one as shown in Figure 3.

$$a(x) = \frac{1}{1 + e^{-x}}$$

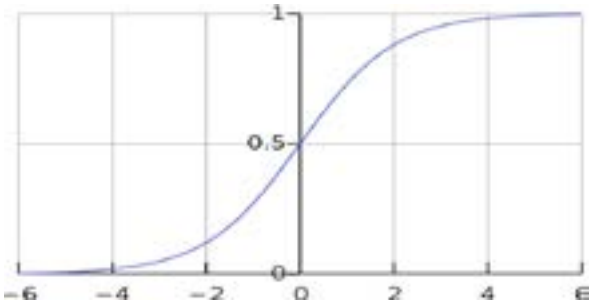

Figure 3. Sigmoid function curve

Hidden layer: the input layer multiplied by sigmoid activation function 1 × 30, where 30 refers to the number of features (neurons) and 1 refers to a BoW vector. It is multiplied by the sigmoid function then MSE (4) is applied in this layer. Output layer: 1 × 642, where 1 means that there is one labeled true question as an output of prediction.MSE is an appropriate choice of error measuring in single hidden layer neural networks, where n is several BoW vectors, y_i is the actual output and y_i is the predicted output. Each actual vector is subtracted from the predicted vector and then squared $(y_i - y_i)^2$. The result is the mean which evaluates the ratio of error.

$$MSE = \frac{1}{n}\sum_{i=1}^{n}(y_i - \hat{y}_i)^2$$

3.RESULT AND DISCUSSION

Figure 4 shows a sample of data that the model trained on. Data used in this approach is a collection of questions about the new disease COVID-19 [16]. The dataset contains 642 questions about COVID-19. The question title is a short

main question with questions about the same subject in different phrasing ways appended to each question title in the question field, in our approach, the question title is trained.

question_id	title	question	answer_id	answer	answer_type	wrong_answer
14057	Can pets catch the cold?	Last night I was drying my cat with a towel af...	14083	Yes they can. The viruses that cause a cold in...	Accepted	That is a Priapulid worm, also known as a "pen...
89709	Is the Common Cold an Immune Overreaction?	It's my understanding that the majority of sym...	89712	Can someone die of the common cold? \n\nNo. \nT...	Accepted	The dash ("-") does not represent a negative c...
89886	Air purifier against bacteria and viruses?	We would buy a mobile air purifier in our home...	89887	The aforementioned filter will filter microbes...	Accepted	It's a bleu ray jellyfish, don't touch is becau...
89929	Why are bats the source of dangerous coronavir...	Why do coronaviruses come from bats?\n\nI mean...	89944	\n The preponderance of links between bat and...	Accepted	First of, depending on your definition of life...
89938	How do bats survive their own coronaviruses?	How do bats survive their own coronaviruses (w...	89975	It's common for the reservoir host of a zoonot...	Accepted	I think that "career in synthetic biology" and...

Figure 4. Sample of dataset visualization

Training is done on the Number of epochs=100 000, 10 000 in each iteration. A large number of epochs makes the error correction higher, time consumed in the training is about 30 minutes on SSD, 12 RAM, i7 core processor PC. Experiments Figure 5 shows the simulation of process flow in the training phase, first the input data "covid1" inputs the model the data converted from nominal to numerical vectors by BoW process then vectors multiplied by the hidden layer input test data in "apply model" state, finally, the output comes out from "performance" phase which is the prediction of a true question then its label-answer-is printed in chatbot as shown in Figure 6:

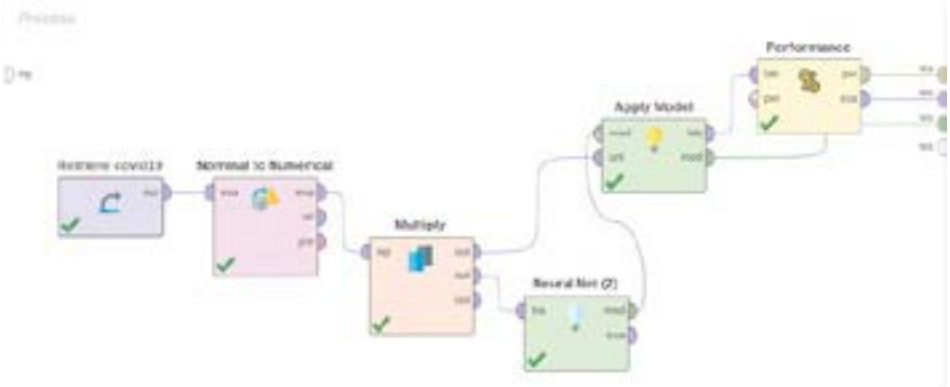

Figure 5. Process visualization of trained model

As shown in Figure 6 the process of NLP must be done before inserting the question of the user into the classifier, after vectorization of the user's input, it is fitted into the classifier, and based on similarity the nearest question from the dataset is chosen to be answered, then the labeled answer is printed in chatbot UI.

GUI Chatbot

Figure 6. Testing the classifier system

Figure 7 shows the chatbot tested with the user, the speed of answering is measured in milliseconds, Table 2 shows the results of the models compared with the ANN BoWs model, as shown the results depend on true or false values, the technique used is the cosine similarity that shows the similarity probability between the predicted question and the questions in the dataset.

Figure 7. Screenshot of our GUI chatbot tested with user

Table 2. Results of models

Question		Prediction result according to model			
		Binary BoW with ANN (our model)	BERT embedding	GloVe embeddingdictionary	TF-IDF BoW
X_actual	Can pets catch the cold?	true	false	true	true
X_prediction	Can dog catch the cold?				

4.CONCLUSION

Chatbots are easy to use and simulate a human conversation through text via smartphones or personal computers. Chatbot applications can improve patient information, monitoring, or treatment adherence. The architecture is a simple neural network consisting of a single hidden layer and the sigmoid function is trained by textual data that is organized by multiple data organization methods. In the final of this paper, the model used is a single layer ANN with BoW text organization method using stemming and tokenization. Results are fairly accepted where the data is not big enough to get high accuracy. The results show that 3 questions are answered true out of 5 questions as the example in Table 2. In future work, the accuracy is planned to be higher, by expanding the neural network to be a deep neural network with more than one hidden layer as well as experimenting with another text organization method such as GloVe embedding dictionary.

REFERENCES

[1] Kumar, A., Meena, P. K., Panda, D., & Sangeetha, Ms. (2019). Chatbot in Python. International Research Journal of Engineering and Technology. Volume 6, issue 11. 391-395. e-ISSN: 2395-0056. https://www.irjet.net/archives/V6/i11/IRJET-V6I1174.pdf .

[2] Park, H., Moon, G., & Kim, K. (2021). Classification of Covid-19 Symptom For Chatbot Using Bert. Advances In Mathematics: Scientific Journal. Volume 10. no.2. 1857-8438 (electronic). ISSN: 1857-8365 (printed). https://doi.org/10.37418/amsj.10.2.34 .

[3] Lei, H., Lu, W., Ji, A., Bertram, E., Gao, P., Jiang, X., & Barman, A. (2021). COVID-19 Smart Chatbot Prototype for Patient Monitoring. arXiv preprint arXiv:2103.06816. https://arxiv.org/abs/2103.06816 .

[4] Höhn S., Bongard-Blanchy K. (2021). Heuristic Evaluation of COVID-19 Chatbots. In: Følstad A. et al. (eds) Chatbot Research and Design. CONVERSATIONS 2020. Lecture Notes in Computer Science, vol 12604. Springer, Cham. https://doi.org/10.1007/978-3-030-68288-09 .

[5] Mikolov, T., Chen, K., Corrado, G., & Dean, J. (2013). Efficient estimation of ord representations in vector space. https://arxiv.org/abs/1301.3781 .

[6] Pennington, J., Socher, R., & Manning, C. (2014). Glove: Global Vectors for Word Representation. EMNLP. 14. 1532-1543. 10.3115/v1/D14-1162, https://doi.org/10.3115/v1/D14-1162.

[7] Joachims T. (1998). Text categorization with Support Vector Machines: Learning with many relevant features. In: Nédellec C., Rouveirol C. (eds) Machine Learning: ECML-98. ECML 1998. Lecture Notes in Computer Science (Lecture Notes in Artificial Intelligence), vol 1398. Springer, Berlin, Heidelberg. https://doi.org/10.1007/BFb0026683.

[8] Harrag, F., El-Qawasmeh, E., & Pichappan, P. (2009). Improving arabic text categorization using decision trees. 110 - 115. 10.1109/NDT.2009.5272214.

[9] Van T. P., Thanh, T. M. (2017). "Vietnamese news classification based on BoW with keywords extraction and neural network," 2017 21st Asia Pacific Symposium on Intelligent and Evolutionary Systems (IES), pp. 43-48, doi: 10.1109/IESYS.2017.8233559.

[10] Sukhbaatar, S., Szlam, A., Weston, J., & Fergus, R. (2015). End-to-end memory networks. arXiv preprint arXiv:1503.08895.

[11] Devlin, J., Chang, M. W., Lee, K., & Toutanova, K. (2018). Bert: Pre-training of deep bidirectional transformers for language understanding. https://arxiv.org/abs/1810.04805 .

[12] Naik, C., Kothari, V., & Rana, Zankhana. (2015). Document Classification using Neural Networks Based on Words. International Journal of Advanced Research in Computer Science. Volume 6, No.2 ISSN: 0976-5697. https://doi.org/10.26483/ijarcs.v6i2.2429 .

[13] Iyer, R., Menon, V., Buice, M,. Koch, C., Mihalas, S. (2013). The Influence of Synaptic Weight Distribution on Neuronal Population Dynamics. PLoS Comput Biol 9(10):e1003248.https://doi.org/10.1371/journal.pcbi.1003248 .

[14] David, E., James, L. M. (1987). "Learning Internal Representations by Error Propagation," in Parallel Distributed Processing: Explorations in the Microstructure of Cognition: Foundations , MIT Press, pp.318-362.

[15] Han, J., Moraga, C. (1995). The influence of the sigmoid function parameters on the speed of backpropagation learning. Lecture Notes in Computer Science, vol 930. Springer, Berlin, Heidelberg. https://doi.org/10.1007/3- 540-59497-3_175.

[16] COVID-19 csv format dataset, https://www.kaggle.com/xhlulu/covidqa . accessed [June 16, 2021].

Research Article

DESIGN AND THRUST/WEIGHT OPTIMIZATION OF A SUPERSONIC PLUG NOZZLE BY TRUNCATION

SIDALI HAIF[1], HAKIM KBAB[1], AMINA BENKHEDDA[1]

[1]Aeronautics and Space Studies Institute, Aeronautical Sciences Laboratory LSA, University of Blida1, Blida, Algeria,haifsidali06@gmail.com, ORCID:0000-0002-9810-761X

ABSTRACT

The popular problem for space propulsion researchers is fuel consumption, which is associated with the weight of the vehicle, and from there, any weight gain leads to fuel gain. We studied the weight reduction of the supersonic nozzle of a space vehicle without any significant effect on the thrust. We first created the contour of theplug nozzle using the method of characteristics, According to the analysis of the pressure profile on the wall of the Plug nozzle we notice that the pressure first decreases very quickly in the initial expansion area, at the level of the col, and continuously decreases in the divergent part before it stabilizes at the tip of the nozzle, approaching the atmospheric pressure value at the outlet of the nozzle. So the last part of the divergent is substantially constant. Therefore, if truncated in this part, this does not lead to a significant decrease in the maximum thrust. In this study, we truncated an ideal supersonic plug nozzle into four different points and we have four Plug nozzles of different lengths and maximum thrust as well. We then choose the Plug nozzle which has an optimized thrust/weight ratio. Finally, we have a Plug nozzle with significant weight gain and a slight maximum thrust loss compared to the ideal plug nozzle.

Keywords: *Method of characteristics, Supersonic plug nozzle.*

1.INTRODUCTION

In this work, we will focus on the plug nozzle study. The plug nozzle is an advanced rocket nozzle that consists of a primary nozzle with a fairly conventional

Received: 08.05.2022 - Accepted: 05.07.2022
DOI: 10.17932/EJEAS.2021.024/ejeas_v02i2004

shape and a plug that allows external expansion. The main characteristics of this nozzle are its interaction with the external environment, which avoids the separation phenomenon that affects a conventional profile nozzle. These advantages derive from the generation of an expansion fan at the lip of the primary nozzle and its influence on the evolution of the pressure along the wall of the plug. The plug nozzle concept was first developed by the Germans prior to World War II for aeronautical applications. Plug nozzles have a central body in the vicinity of the neck and the process of gas expansion is directly or indirectly regulated by ambient pressure, the gas flow is regulated by detent waves from the flow deviation due to the plug surface [1]. Based on weight/push ratio considerations, the cap is generally truncated, resulting in a very complex base flow. The use of these nozzles in the past is very rare, for example the Second World War fighter aircraft named Messerschmitt Me 262 was equipped with an annular plug nozzle. For the first time in 1950 Griffith of Rolls-Royce, Ltd is proposed the concept of a plug nozzle for rocket propulsion in an American patent [2]. In 1959, Krase was the first to propose methods to designate ideal plug nozzle contours by simple approximate calculations [3]. In 1961 Berman and Cromp made studies on the modification of the end of plug and they obtained that if one uses half-cone angles at the end of the plug one has a decrease in performance of only 1% [4]. In the same year Rao discussed the use of plug contour optimization as the case in the conventional nozzle and obtained optimal contours [5]. In 1964, Angelino described an approximate method for axisymmetrical and two-dimensional plug nozzle design based on a simple technique [6]. Balasaygun studied the deference of performance between the plug nozzles and the Conventional nozzles, he obtained that the nature of the flow in the plug nozzles is auto-adjustable to allow it when operating at a pressure ratio lower than a design ratio to obtain a thrust advantage over a conventional nozzle [7]. In 1974, Johnson and al presented an optimization analysis for axial plug nozzles with variable input geometry [8]. In 1997, Rommel and al studied the development of the flow field as a function of ambient pressure variations using a computer study of a plug nozzle [9]. To minimize weight McConnaughey conducted a numerical study of a three-dimensional aerospike and concluded that a 50% truncation of the plug nozzle resulted in a 0.5% reduction in performance only [10]. In 1998, Hagemann G and al carried out a numerical study based on the method of characteristics for the flow field simulations of plug nozzles, and they discussed the flow phenomena observed in experiments and numerical simulations of different adaptive plug nozzles in altitude [11]. In 2002, Ito and Al studied flow structures and thrust performance of axisymmetric trancated plug nozzles using a numerical simulation, they obtained a high gain from the plane plug nozzle (aerospike) of about 5 to 6% compared to the axisymmetric plug nozzle and for pressure ratios greater than the design ratio the pressure distribution on the nozzle wall was not affected

by the external flow [12]. Besnard and al presented the manufacture, design, and testing of a thrust engine equal to 1000 lbf of plug nozzle type, the results showed that variations in heat capacity ratio led to a difference in thrust characteristics [13]. In 2006, Zebbiche plotted the profiles of the plug nozzle on the use of the Prandtl Meyer function for several forms by changing the ratio of specific gamma heat and comparing the performance of the plug nozzle compared to an MLN nozzle. Performance is better compared to MLN [14]. In 2010, Shahrokhi and Noori used CFD to study the deferential flow properties of the Aerospike nozzle [15]. In 2012, Karthikeyan. N and Al studied the effect of plug truncation of an aerospike nozzle on acoustic behavior [16]. In 2014, Chutkey and Al conducted a numerical and experimental study on the behavior of flow fields at truncated annular plug nozzle of different lengths [17]. In 2015, Shanmuganathan and Al conducted a numerical comparative study on linear and annular plug nozzles and obtainedthat the annular nozzle was better than the linear nozzles [18]. In 2017, Kumar, N. and All compared the full length to the optimized plug nozzle models and discussed the aerospike nozzle design procedure and the parameters governing its design [19].

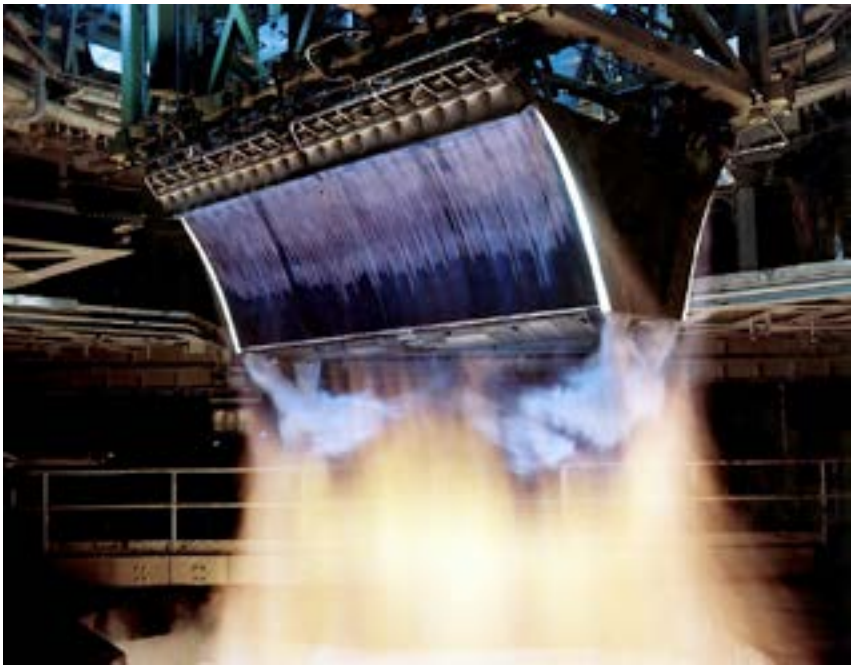

Figure1. Picture of the Plug nozzle from Wikipedia

2.THEORY

A FORTRAN program was created based on the characteristic method that was described in the reference [14]. In mathematics, the method of characteristics is a technique for solving partial differential equations. The characteristic method applied to the two-dimensional isentropic flow of an ideal gas is used for the design of supersonic nozzles which produce a uniform parallel flow at the outlet of the nozzle. The program designed the contour of the bi-dimensional supersonic plug nozzle. The design method is based on the function of Prandtl Meyer.

(1)

$$\nu(M) = \left(\frac{\gamma+1}{\gamma-1}\right)^{\frac{1}{2}} \tan^{-1}\left[\frac{\gamma-1}{\gamma+1}(M_e^2-1)\right]^{\frac{1}{2}} - \tan^{-1}(M_e^2-1)^{\frac{1}{2}}$$

The number of Mach M = 1.00 at the col and accelerates to the Mach number M_E at the exit section. v Is the angle between the velocity vector of the col and the x-axis. The lines shown in figure 1 represent the Mach waves, they are inclined with an angle u, and the flow properties are constant along each line of Mach exits from point A.

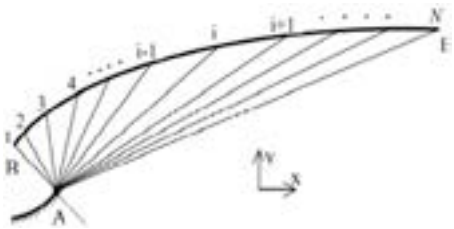

Figure 2. Discretization of the expansion zone

The main idea of this method is considered the velocity vector as the contour of the required plug wall, the latter is tangent to the current line. To have a Mach number required at the exit, the flow to the col must be tilted at an angle 0_B .

$$0_B = (M_E)$$

(2)

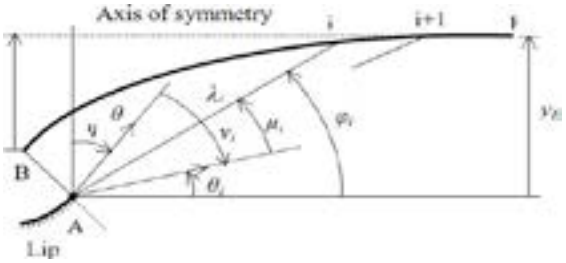

Figure 3. Parameters of an intermediate Mach

The determination of wall points is made explicitly. The lines are iso-Mach curves, so the number of Mach in the center of expansion A equals also the number of Mach on the wall. The number of Mach in point i is given by:

$$M_i = 1 + (i - 1)\left[\frac{M_E - 1}{N - 1}\right] \quad (i = 1,2,3, \dots, N) \qquad (3)$$

With N is the selected point number.
Once the number of Mach M_i in point i is known. In this case we can write:

$$u_i = \sin^{-1}\left(\frac{1}{M_i}\right) \qquad (4)$$

$$v_i = v(M_i) \qquad (5)$$

$$\theta_i = \varphi_i - u_i \qquad (6)$$

$$\frac{x_{i+1}}{\lambda_a} = \left(\frac{\lambda_{i+1}}{\lambda_a}\right)\cos\varphi_{i+1} \qquad (7)$$

$$\frac{y_{i+1}}{\lambda_a} = \left(\frac{\lambda_{i+1}}{\lambda_a}\right)\sin\varphi_{i+1} \qquad (8)$$

$$\frac{\lambda_{i+1}}{\lambda_a} = \left(\frac{\lambda_i}{\lambda_a}\right)\frac{\sin\alpha}{\sin\beta} \qquad (9)$$

$$\alpha = \pi - \varphi_i + v_E - v_i \qquad (10)$$

$$\beta = \varphi_{i+1} - v_E + v_i \qquad (11)$$

3.RESULTS AND DISCUSSION

To start the calculation of the program. Give some values among them M_E (number of Mach at the exit) and y (Adiabatic Gas Index) and N (selected point number). The outputs of this program are a set of x and y coordinates that represent the contour of the nozzle. In this study, we based on the following data :

$M_E = 2,4$

$y = 1,4$

$N = 1200000$

Figure 4 above, Illustrates the profile obtained for the plug nozzle with $M_E = 2,4$ and $y = 1,4$.All the geometric characteristics of the designed nozzle are shown in Table 1.

Table 1. Geometrical data of the plug nozzle profile

Quantities	**Values**
Throat radius yt , *m*	0,010
Nozzle length L, *m*	0,052
Nozzle area *S*, m^2	0,062
Area ratio Æt / Æe	0,420

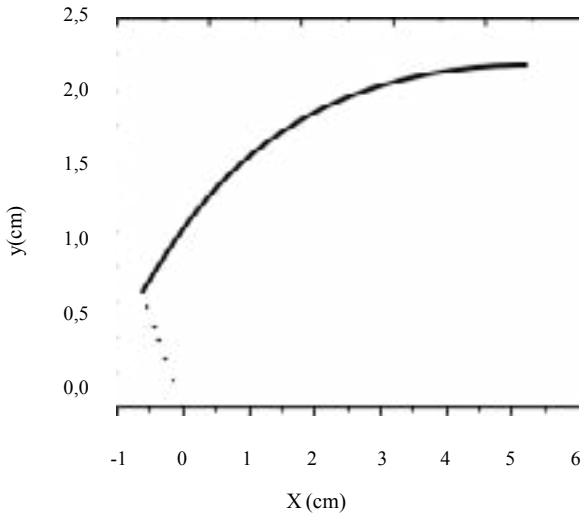

Figure 4. Shapes of the plug nozzle when M_E = 2,4 and y = 1,4

For the validation of the program, we have a numerical simulation of flows in the obtained plug nozzles achieved using the computer code ANSYS. The table 2 groups the thermodynamic data used during our calculations to draw the profile of the plug nozzle.

Table 2. Thermodynamic data of the plug nozzle profile

Quantities	**Values**
Chamber temperature T_C, *K*	300
Chamber pressure P_t, *Bars*	2,00
Design Mach number M_e	2,40
Ambient pressure $P_Æ$, *Bars*	0,14
Specific heat ratio *Y*	1,40

Figure 5 shows the Iso-Pressure contours for a plug nozzle that works in the design Mach number obtained by our simulation, the figure appears the Prandtl–Meyer expansion fan around the lip.

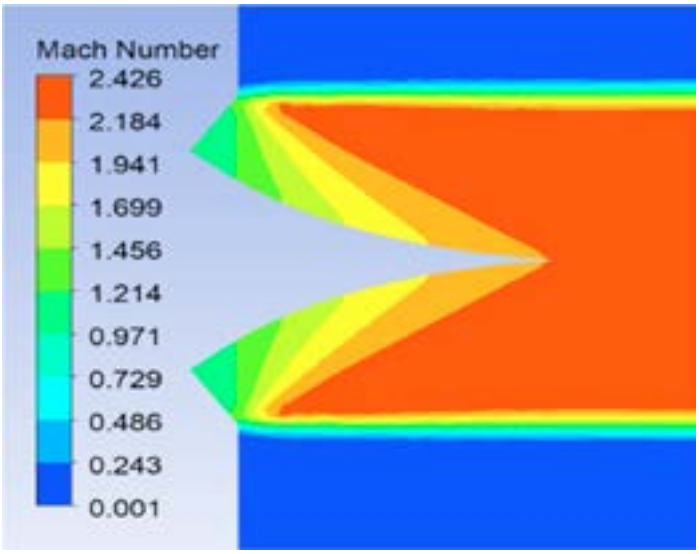

Figure 5. Iso-pressure contours

Figure 6 represents the evolution of the Mach number along the wall of the plug nozzle. We note that in the divergent part, the number of Mach increases until reaching the value of the nozzle designing Mach number at the outlet.

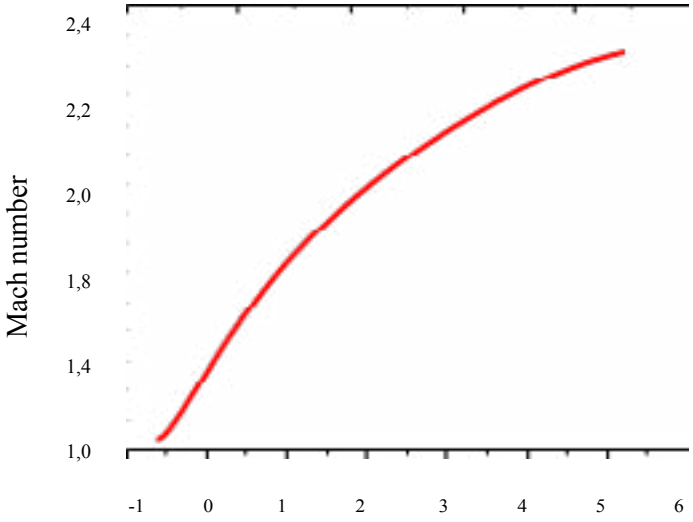

Figure 6. Wall Mach evolution

Figure 7 shows the wall static pressure obtained by the simulation for M_E = 2.4. According to the analysis of the pressure profile on the wall of the nozzle we notice that the pressure first decreases very quickly in the initial expansion area, at the level of the col, and continuously decreases in the divergent part before it stabilizes at the tip of the nozzle, approaching the atmospheric pressure value at the outlet of the nozzle. So the last part of the divergent is substantially constant. Therefore, if truncated in this part, this does not lead to a significant decrease in the maximum thrust. In this study, we truncated an ideal supersonic nozzle into four different points, as figure 8 shows.

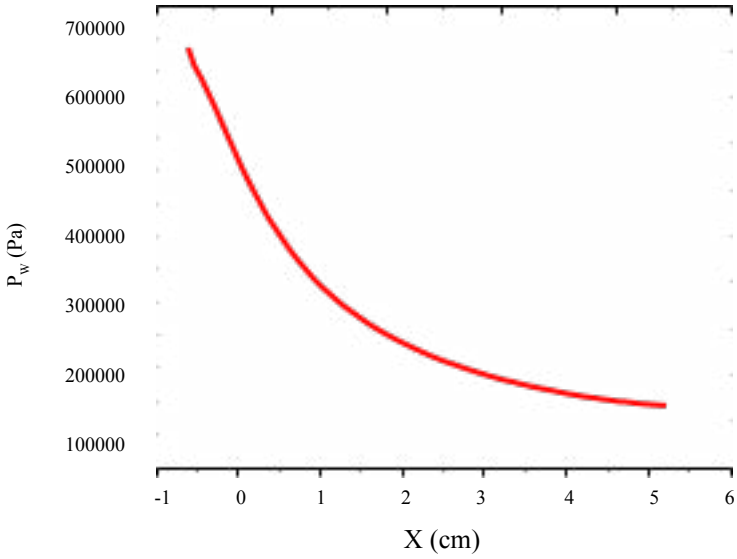

Figure 7. Wall pressure evolution

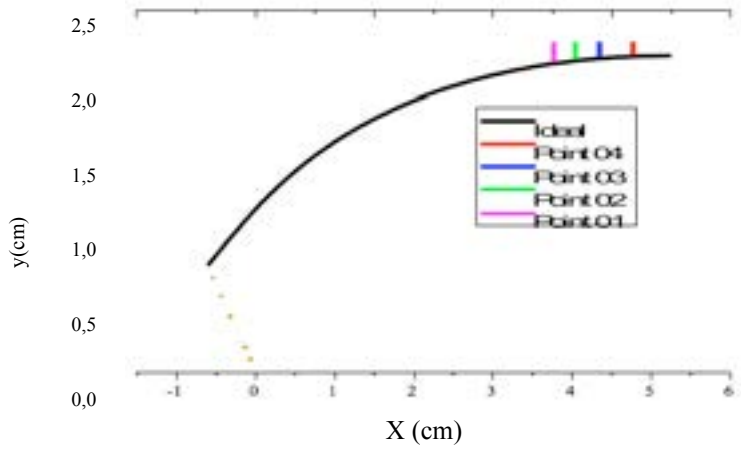

Figure 8. Truncated profil

Table 3. Truncated point

	Point 01	Point 02	Point 03	Point 04	ideal
Thrust (N)	9246,07	9328,47	9397,47	9496,21	9706,15
Mach in the exit	2,20	2,25	2,29	2,34	2,40
Length (cm)	3,77	4,05	4,35	4,78	5,24
Surface (m2)	0,0475	0,0499	0,0529	0,0572	0,0618
Loss of thrust%	4,74	3,89	3,18	2,16	/
Weightloss %	23,14	19,26	14,40	7,44	/
Thrust/ Weight	0,186	0,202	0.22	0.29	/

Table 3 summarizes the truncated nozzle performances in terms of thrust, Mach in the exit, Length, Surface, Loss of thrust, and Loss of weight for four truncation points whose abscissas are: 3,77 cm 4,05 cm 4,35 cm, and 4,78 cm respectively. It is noticed that for truncation in point 2, the thrust losses are equal to 3,89%. On the other hand, the gain concerning the Surface is about 19,26% which will affect the weight of the nozzle.

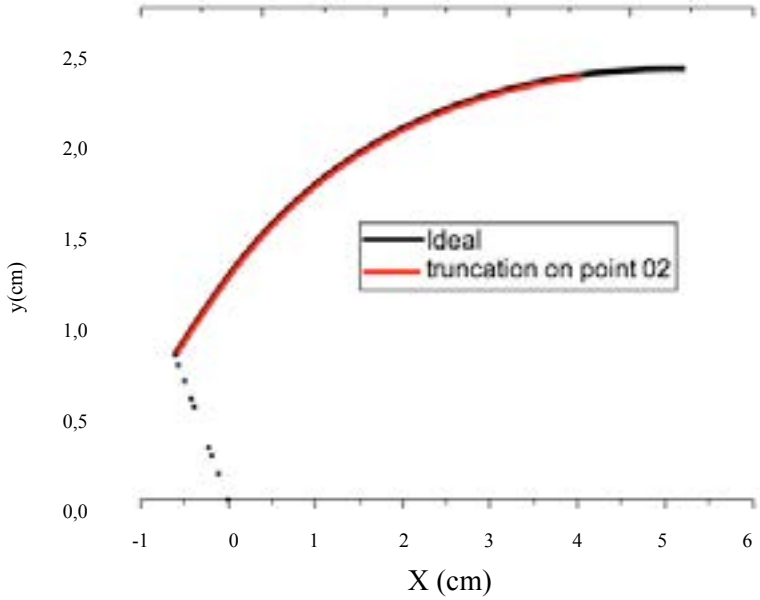

Figure 9. The difference of ideal and truncated profile

4.CONCLUSION

We do truncations on the last part of the divergent in 4 different points. After the truncation of the ideal nozzle, we calculate the thrust, the number of Mach at the Exit, the length, and the area. We use the area variable to express weight. And for the sake of comparison, we calculate the Thrust Loss, Weight Loss, and the Thrust / Weight ratio. We then choose the plug nozzle which has an optimized thrust / weight ratio. Finally, we have a plug nozzle with a weight gain equal to 19,26% and a thrust loss of only 3,89%.

REFERENCES

[1] Hagemann, G., et al., Advanced rocket nozzles. Journal of Propulsion and Power, 1998. 14(5): p. 620-634.

[2] Arnold, G.A., Jet-propulsion nozzle for use at supersonic jet velocities, 1954, Google Patents.

[3] Krase, W., Performance analysis of plug nozzles for turbojet and rocket exhausts. Vol. 79962. 1959:American Society of Mechanical Engineers.

[4] Herman, K. and F. Crimp Jr, Performance of plug-type rocket exhaust nozzles. ARS Journal, 1961. 31(1): p. 18-23.

[5] Rao, G., Spike nozzle contour for optimum thrust. Planetary and Space Science, 1961. 4: p. 92-101.

[6] ANGELINO, G., Approximate method for plug nozzle design. AIAA Journal, 1964. 2(10): p. 1834-1835.

[7] Balasaygun, E., Experimental analysis of plug nozzles. 1964.

[8] Johnson, G.R., H.D. Thompson, and J.D. Hoffman, Design of maximum thrust plug nozzles with variable inlet geometry. Computers & Fluids, 1974. 2(2): p. 173-190.

[9] Rommel, T., et al., Plug nozzle flowfield analysis. Journal of Propulsion and Power, 1997. 13(5): p. 629-634.

[10] Ruf, J. and P. McConaughey. A numerical analysis of a three dimensional aerospike. in 33rd JointPropulsion Conference and Exhibit. 1997.

[11] Hagemann, G., H. Immich, and M. Terhardt. Flow phenomena in advanced rocket nozzles-the plug nozzle.in 34th AIAA/ASME/SAE/ASEE Joint Propulsion Conference and Exhibit. 1998

[12] Ito, T., K. Fujii, and A.K. Hayashi, Computations of axisymmetric plug-nozzle flowfields: Flow structures and thrust performance. Journal of Propulsion and Power, 2002. 18(2): p. 254-260.

[13] Besnard, E., et al. Design, manufacturing and test of a plug nozzle rocket engine. in 38thAIAA/ASME/SAE/ASEE Joint Propulsion Conference & Exhibit. 2002.

[14] Zebbiche, T. Supersonic plug nozzle design. in 41st AIAA/ASME/SAE/ASEE Joint Propulsion Conference & Exhibit. 2005.

[15] Shahrokhi, A. and S. Noori. Survey of the central plug shape of the aerospike nozzle. in 17th AustralasianFluid Mechanics Conference, Auckland, New Zealand. 2010.

[16] Karthikeyan, N., et al., Effect of spike truncation on the acoustic behavior of annular aerospike nozzles. AIAA Journal, 2013. 51(9): p. 2168-2182.

[17] Chutkey, K., B. Vasudevan, and N. Balakrishnan, Analysis of annular plug nozzle flowfield. Journal ofspacecraft and rockets, 2014. 51(2): p. 478-490.

[18] Shanmuganathan, V., et al., Comparative study on performance of linear and annular aero-spike nozzles. Aust J Basic Appl Sci, 2015. 9(11): p. 883-892.

[19] Kumar, K.N., et al. Design and Optimization of Aerospike nozzle using CFD. in IOP Conference Series: Materials Science and Engineering. 2017. IOP Publishing.

Research Article

NUMERICAL ANALYSIS ON HEAT TRANSFER AND FLOW CHARACTERISTICTHROUGH ELLIPTICAL TWISTED TUBE

TOYGUN DAGDEVİR[1]

[1] Department of Mechanical Engineering, Erciyes University, Kayseri, Turkey
**E-mail address: toygun@erciyes.edu.tr,*
ORCID: 0000-0001-7388-3391

ABSTRACT

In the present study, a circular smooth tube (CST), an elliptical smooth tube (EST) and various elliptical twisted tube (ETT) configurations are investigated according to heat transfer and flow characteristics by using a CFD software. The ETT configurations are considered as the aspect ratio (AR) of 1.5 and 2.0 and the twist pitch length (PL) of 50, 100 and 200 mm. The hydraulic diameter of the tubes is kept constant to ensure that the results are independentof the hydraulic diameter size. A constant heat flux of 50 kW/m^2 is applied to the test tube and the flow conditions are under turbulent flow conditions corresponding to Reynolds number 4060-26,998. Water is elected as a working fluid. The thermal and physical properties of the fluid are considered dependent on temperature. It is resulted that the ETT contributes to enhancing heat transfer, despite increasing the friction factor. As the AR increases and the PL decreases, the heat transfer is positively affected, while the friction factor is negatively affected. As a result, when the heat transfer and the hydraulic performance of all cases are simultaneously determined with the performance evaluation criteria (PEC) value, the highest PEC value is obtained as 1.39 for the case of ETT_AR=2.0_PL=50 at Reynolds number of 4524.

Keywords: *Heat transfer, flow characteristic, elliptical twisted tube, numerical analysis.*

1.INTRODUCTION

Due to rapidly increasing the population and running out of fossil fuels, the energy need has been increasing day by day. In this respect, it will be always valuable to use the energy efficiently. Since most of the engineering applications in the industry involve heat exchangers, studies aimed at increasing the efficiency of

Received: 18.02.2022 - Accepted: 08.06.2022
DOI: 10.17932/EJEAS.2021.024/ejeas_v02i2005

heat exchangers are important in terms of the energy efficiency. In addition, with increasing the efficiency of heat exchangers, smaller scale heat exchangers can be designed. Heat transfer enhancement techniques are divided into two techniques: active technique and passive technique. Active techniques require extra power for the system, while passive techniques do not require any power input to the system [1]. The passive techniques consist of using turbulator devices in the tube such as twisted tape [2,3] and coiled wire [4,5], extending surfaces [6] of the tube as corrugated tube [7], coiled tube [8], placing pin fins [9] and twisted tubes [10,11] and using nanofluid [12,13].

Dong et al. [14] experimentally investigated the thermal and hydraulic performance of the spiral twisted tube. Their results showed that the spirally twisted tube heat exchangers provide obvious heat transfer enhancement for both the laminar and the turbulent flow. They also present heat transfer correlations for the spiral tube heat exchanger with a deviation of ±10%. Yu et al. [10] investigated the turbulent heat transfer performance of twisted oval tubes with different cross-sectioned wire coil inserts. Their results show that using twisted tube and wire coil together could further enhance heat transfer rate and pump consumption, while the performance evaluation criteria decreased. Tan et al. [11] conductedan experimental study on twisted oval tube heat exchanger. They recommended that the twisted oval tube heat exchangers are to work at low tube side flow rate and high shell side flow rate. Tang et al. [15] experimentally and numerically investigated the circular tube, elliptical twisted tube and tri-lobed tube using water fluid with respect to thermal and hydraulic performance. They resulted in the twisted tri-lobed tube that is more suitable for substituting for a straight tube in heat exchanger according to performance evaluation criteria.

In the light of the literature review cited above, the twisted tube is a good choice to increase the heat transfer performance of the heat exchangers. However, an assessment on the aspect ratio (AR) and twist pitch length (PL) have not been presented yet according to heat transfer performance, flow characteristic and performance evaluation criteria.

With this motivation, a numerical study is carried out to investigate the effects of the AR and the PL on the heat transfer, the flow characteristic and performance evaluation criteria.

2.MATERIAL AND METHODOLOGY

2.1.PHYSICAL MODEL

In this study, a circular smooth tube (CST), an elliptical smooth tube (EST) and various configurated elliptical twisted tubes (ETT) are considered to investigate the heat transfer and flow characteristic. The ETTs are configurated with a dif-

ferent aspect ratios (AR) of 1.5 and 2.0 and twist pitch lengths (PL) of 50, 100 and 200 mm. The considered tubes are illustrated in Figure 1. The dimensions of the ellipse (a and b) are adjusted to keep the hydraulic diameter of 17 mm constant so that the hydraulic diameter does not affect the non-dimensional number such as Nusselt number (Nu), friction factor (f) and performance evaluation criteria (PEC). The solution domain consisting of main three sections: an entrance section, a test section and an exit section is depicted in Figure 2. In order to provide the hydraulic developed flow, the entrance tube before the test section which is a length of 1000 mm is placed with length of 250 mm [16]. The exit section with a length of 150 mm is placed to prevent the reserve flow effects.

Figure 1. Considered tube configurations in the study

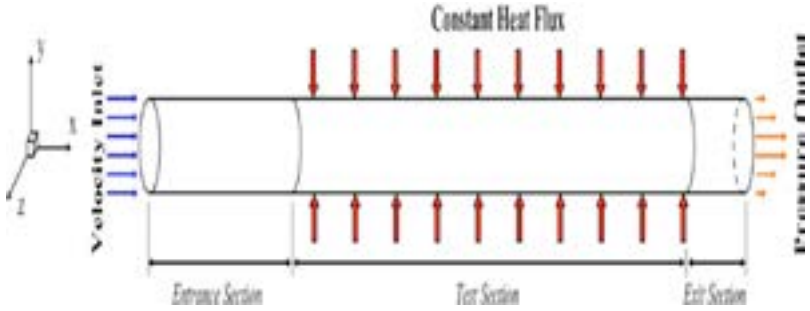

Figure 2. Solution domain with boundary typest

2.2.NUMERICAL METHOD

The thermal and hydraulic performance of the considered tubes are numerically investigated by using a CFD program. k-ω, the Standard turbulence model is used to simulate turbulent flow through the solution domain. Polyhedral mesh structure with boundary layer mesh is generated for the solution domain as shown in Figure 3.

Figure 3. Used mesh structure for the numerical analysis

2.3.GOVERNING EQUATIONS

The CFD program solves continuity (1), momentum (2) and energy (3) conservation equations [17].

$$\nabla(\rho\vec{V}) = 0 \tag{1}$$

$$\nabla(\rho\vec{V}\vec{V}) = -\Delta P + \nabla(\mu\nabla\vec{V}) \tag{2}$$

$$\nabla(\rho c_p\vec{V}T) = \nabla(k\nabla T) \tag{3}$$

Where ρ is fluid density, V is velocity, P is pressure, μ is dynamic viscosity,capacity, k is thermal conductivity, and T is temperature.

Semi Implicit Method for Pressure Linked Equations (SIMPLE) algorithm scheme is conducted to achieve the relationship between pressure and velocity coupling to enforce mass conservation and to obtain pressure field [17]. Quadratic Upstream Interpolation for Convective Kinematics (QUICK) scheme is used for discretion of convection terms and diffusion terms. The residual criteria of continuity, velocities, energy, k and ω are taken as $1 \times 10{-}5$ to ensure convergence of the solution.

$$\frac{\partial}{\partial t}(\rho k) + \frac{\partial}{\partial x_i}(\rho k V_i) = \frac{\partial}{\partial x_j}\left(\Gamma_k \frac{\partial k}{\partial x_j}\right) + G_k - Y_k + S_k \tag{4}$$

$$\frac{\partial}{\partial t}(\rho \omega) + \frac{\partial}{\partial x_i}(\rho \omega V_i) = \frac{\partial}{\partial x_j}\left(\Gamma_\omega \frac{\partial \omega}{\partial x_j}\right) + G_\omega - Y_\omega + S_\omega \tag{5}$$

In these equations, G_k represents the generation of turbulence kinetic energy due to the mean velocity gradients. G_ω is the generation of ω. Γ_k and Γ represent the effective diffusivity of k and ω, respectively. Y_k and Y_ω represent the dissipation of k and ω due to turbulence. All of the above terms are calculated as described below. S_k and S_ω are user-defined source terms. The effective diffusivities for the k- ω model are given by.

$$r_k = \mu + \frac{\mu_t}{\sigma_k} \quad (6)$$

$$r_w = \mu + \frac{\mu_t}{\sigma_w} \quad (7)$$

Where σ_k and σ_ω are the turbulent Prandtl numbers for k and ω, respectively. The turbulent viscosity,
μ_t, is computed by combining k and ω as follows. a^* is assumed as 1.0 in the high Reynolds number formof the k-ω model equations. Detailed information is available in the Fluent user guide [17].

$$\mu_t = \alpha^* \frac{\rho k}{\omega} \quad (8)$$

2.4. DATA REDUCTION

Used data are exported from the software with area-weighted average by using surface integrals.The Reynolds number (Re), which is a ratio of inertial force to viscous force, is expressed as:

$$Re = \frac{\rho D_h V}{\mu} \quad (9)$$

where ρ density of the fluid, D_h is the hydraulic diameter of the tube, V velocity of the fluid and μ the is dynamic viscosity of the fluid.
The average Nusselt number (Nu), which is ratio of convective heat transfer rate to conductive heattransfer rate, is expressed as:

$$Nu = \frac{h D_h}{k} \quad (10)$$

k is thermal conductivity of the fluid, and the average convective heat transfer coefficient (h)along the test section is calculated as:

$$h = \frac{q}{\Delta T} \quad (11)$$

q is constant heat flux applied onto the wall surface of the entrance and test section. The averagetemperature difference (ΔT) in this equation is expressed as:

$$\Delta T = T_s - T_b \tag{12}$$

where T_S is wall surface of the test section temperature and T_b is the fluid bulk temperature between inlet and outlet of the test section. The friction factor (f) defined by Fanning friction factor is expressed as:

$$f = \frac{\Delta T}{1/2\rho V^2 \frac{L}{D_h}} \tag{13}$$

where ΔP is the pressure difference between inlet and outlet of the test section. L is the length of the test section of the tube. Performance evaluation criteria (PEC) is used to evaluate heat transfer performance and hydraulic characteristics with Eq. (14) at the same Re number.

$$PEC = \frac{Nu/Nu_0}{(f/f_0)^{1/3}} \tag{14}$$

where Nu_0 and f_0 represent the Nusselt number and friction factor of the non-applied any passiveheat transfer enhancement technique, respectively.

3.RESULTS AND DISCUSSION

3.1.VALIDATION OF NUMERICAL METHODOLOGY

The validation of the numerical methodology should be ensured to prove the accuracy of the study. In this scope, the validation of the study for the (CST) is obtained according to the Nusselt number and the friction factor versus Reynolds number as given in Figure 4 by comparing Dittus and Boelter equation [18] and Blasius equation [19]. Obtained maximum deviations from the validation study are approximately ± 3.59% and ± 12.93% for the Nusselt number and the friction factor, respectively.

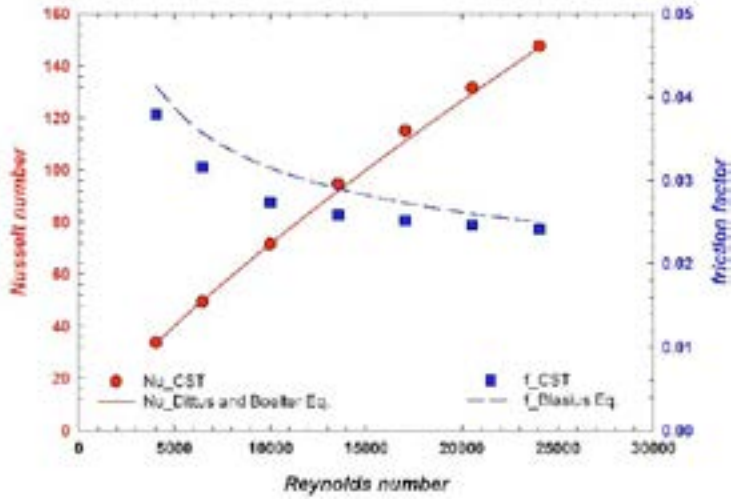

Figure 4. Validation of CST for both the Nusselt number and the friction factor versus the Reynolds number

3.2.RESULTS OF THE NUMERICAL STUDIES

In this study, the effect of the AR and the PL of the ETT is numerically investigated on the heat transfer, flow characteristics and PEC. The AR is adjusted as 1.5 and 2.0 by keeping constant the hydraulic diameter of 17.0 mm which belongs to the CST. The ETTs are created to have PL of 50, 100 and 200 mm.

3.3.HEAT TRANSFER

Nusselt number is used to interpret the heat transfer performance of the heat exchanger tube. Fig. 5 shows the distribution of Nusselt number results with respect to Reynolds number for all considered tube configurations. As widely known, as the Reynolds number increases the Nusselt number increases for all cases, since the turbulent flow plays a major role in enhancing the convective heat transfer rate in the internal tube flow.

It is clearly seen from Fig. 5 that the increase in the AR leads to an increase the Nusselt number for all Reynolds numbers. The reason of this result is the fact that as the AR increase, the diameter of the ETT is shrunk. This phenomenon leads to thin the thickness of the thermal boundary layer.

When the heat transfer performance of the ETT is examined in terms of the PL, as the PL decreases, the Nu increases for all Reynolds numbers. One of the reasons

for this result is the decrease in the PL means to increase in the surface area of the ETT. As expected, the heat transfer surface area is directly proportional to the convective heat transfer. Another reason for that is as the PL decreases through the tube, the tendency of the disrupted boundary layers to affect each other has increased. As a result, the decrease in the PL inclines both to increase the heat transfer surface area and to disrupt the thermal boundary layer more.

The statements mentioned above can be supported by Fig. 6 where the temperature contours for all considered tube cases are shown. It is seen from the figure that the thermal boundary layer is disrupted and the bulk temperature is higher for the case having a higher Nusselt number result than the others. For instance, a zone having a minimum temperature that is 300 K is not observed for the ETT_AR=2.0_PL=50, while as the PL increases for the other cases, the zone having a minimum temperature expands. Furthermore, it is seen the intensification of the secondary flow from Fig.8. The secondary flow is another phenomenon causing to enhances the convective heat transfer. The velocity gradient at the cross-sectional area of the tube is observed in the Fig. 8. The more irregular velocity gradient occurs at the secondary flow, the fluid is more severely mixed. Therefore, it serves to enhance the convective heat transfer.

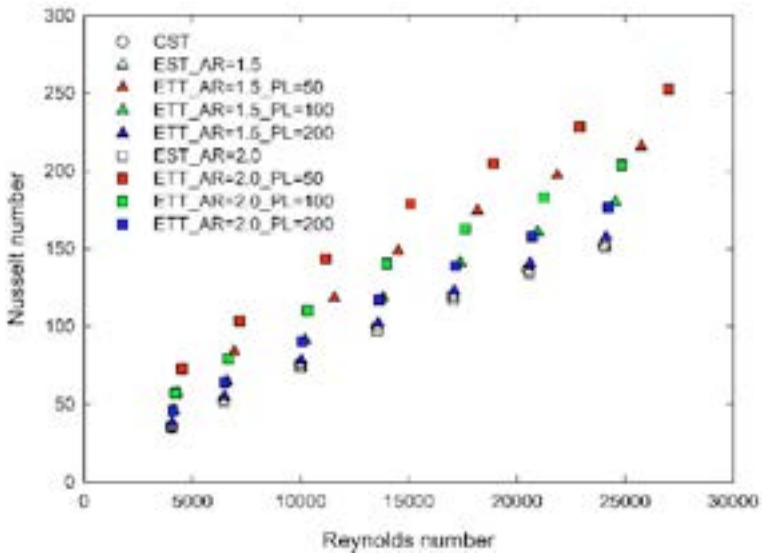

Figure 5. Distribution of Nusselt number results versus the Reynolds number

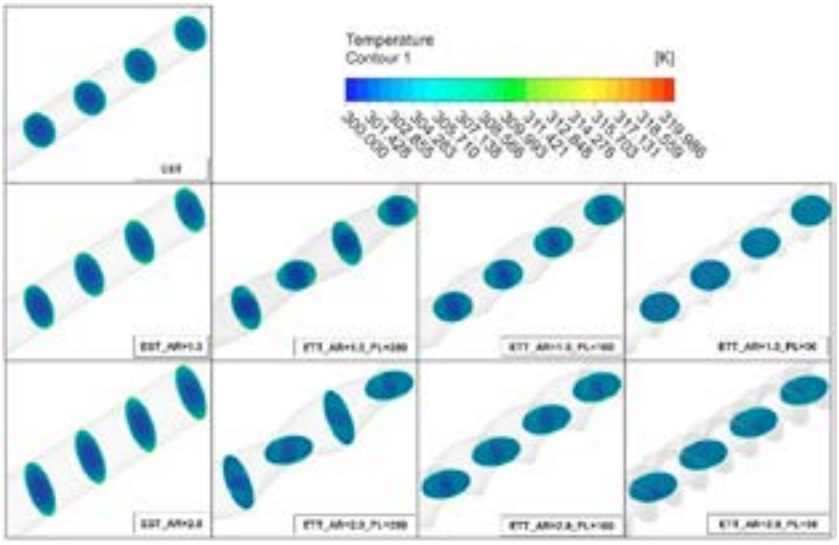

Figure 6. Temperature contours at different cross-sectional areas for the all cases at Reynolds number of 14,000.

3.4.FLOW CHARACTERISTIC

Friction factor (f) is used to discuss and interpret the flow characteristic occurring through the considered tube cases. Fig. 7 shows the distribution of friction factor results with respect to Reynolds number for the cases. It is widely known that as the Reynolds number increases, the friction factor decreases for the internal tube flow. Because, the inertial forces are dominant on the viscous forces adjacent the inner surface of the tube. The highest friction factor result is observed for the case of ETT_AR=2.0_PL=50 for all Reynolds numbers. There is a directly proportional among the various PL which is that as the PL decreases the friction factor increases since the size of the obstacle surface area increases through the ETT.

Moreover, as the AR increases, the friction factor increases. It is because the velocity magnitude increase and the pressure drop increases when the tube section is shrunk.

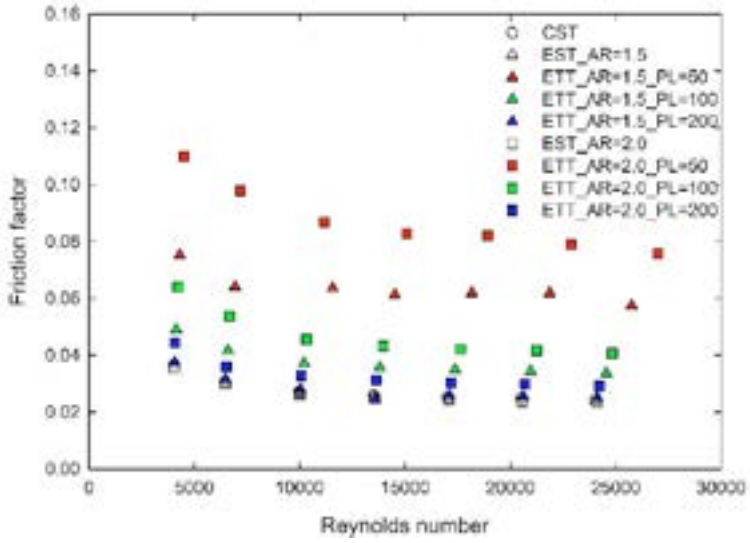

Figure 7. Distribution of friction factor results versus the Reynolds number

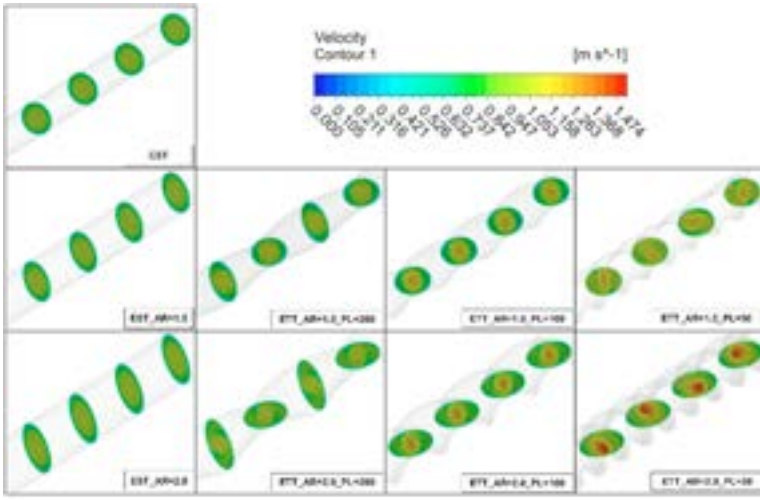

Figure 8. Velocity contours at different cross-sectional areas for the all cases

In addition to the results mentioned above, it should be emphasized that the kept the hydraulic diameter constant does not cause severe effects for neither the Nusselt number nor the friction factor. Therefore, comparing the ETTs having various AR and PL with each other is sensible and acceptable.

3.5.PERFORMANCE EVALUATION CRITERIA

Performance evaluation criteria (PEC) is widely used to determine the performance of the heat exchangers in terms of both heat transfer and hydraulic performance, simultaneously. It is accepted that if the PEC value is higher than 1.0, the case is beneficial to employ the related case in the application. For this purpose, Fig. 9 is given to compare the PEC results obtained from the considered cases versus the Reynolds number. It is resulted that the highest PEC value is obtained as 1.39 from the case of ETT_AR=2.0_PL=50 at a Reynolds number of approximately 4524. The second high PEC value is obtained from the case of ETT_AR=2.0_PL=100. It shows that the AR has more effect than PL on the PEC. It is because the increase in the heat transfer is greater than the decrease in the friction factor when the AR and the PL is compared with each other.

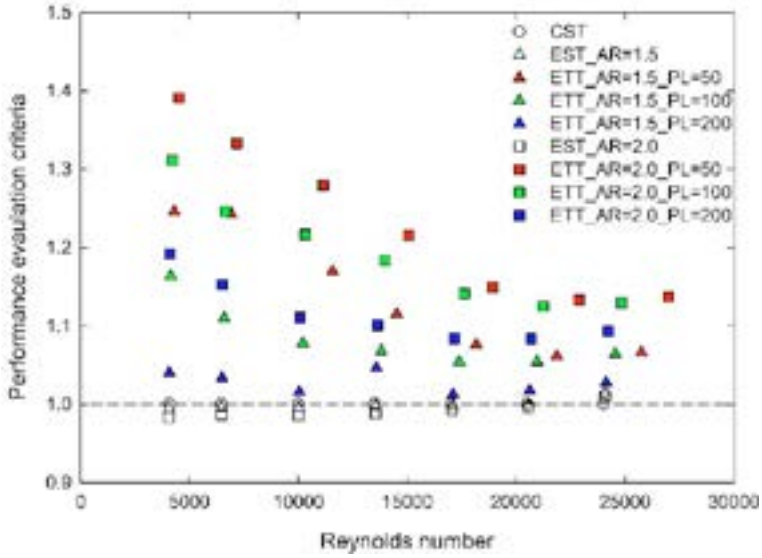

Figure 9. Distribution of performance evaluation criteria results versus the Reynolds number

4.CONCLUSION

This study presents a numerical study investigating the effects of the aspect ratio (AR) and the pitch length (PL) of the elliptical twisted tube (ETT) on heat transfer, flow characteristics and performance evaluation criteria (PEC). All tube cases are considered by keeping the hydraulic diameter constant. The flow conditions are turbulent corresponding the Reynolds number ranging from approximately 5000 to 25,000. Revealed conclusions from the study are given in the followings:

1. When the hydraulic diameter is kept constant for the ETTs, the Nusselt number, the friction factor and the PEC are not severely affected.
2. The increase in the AR leads to an increase in the Nu, the f and the PEC for all Reynolds numbers.
3. The decrease in the PL leads to an increase in the Nu, the f and the PEC for all Reynolds numbers.
4. The highest Nu is obtained as 252.52 at Re of 26998 for ETT_AR=2.0_PL=50. At the same time, the highest Nu corresponds to 1.5 times the smooth tube at the same the Re.
5. The highest PEC value is obtained as 1.39 for ETT_AR=2.0_PL=50 at Re of 4524.

REFERENCES

[1] Sidik NAC, Muhamad MNAW, Japar WMAA, Rasid ZA. An overview of passive techniques for heat transfer augmentation in microchannel heat sink. Int Commun Heat Mass Transf 2017;88:74–83. https://doi.org/10.1016/J.ICHEATMASSTRANSFER.2017.08.009.

[2] Varun, Garg MO, Nautiyal H, Khurana S, Shukla MK. Heat transfer augmentation using twisted tape inserts: A review. Renew Sustain Energy Rev 2016;63:193–225. https://doi.org/10.1016/J.RSER.2016.04.051.

[3] Dagdevir T, Ozceyhan V. An experimental study on heat transfer enhancement and flow characteristics of a tube with plain, perforated and dimpled twisted tape inserts. Int J Therm Sci 2021;159:106564. https://doi.org/10.1016/j.ijthermalsci.2020.106564.

[4] Sheikholeslami M, Gorji-Bandpy M, Ganji DD. Review of heat transfer enhancement methods: Focus on passive methods using swirl flow devices. Renew Sustain Energy Rev 2015;49:444–69. https://doi.org/10.1016/J.RSER.2015.04.113.

[5] Gunes S, Ozceyhan V, Buyukalaca O. Heat transfer enhancement in a tube with equilateral triangle cross sectioned coiled wire inserts. Exp Therm Fluid Sci 2010;34:684–91. https://doi.org/10.1016/J.EXPTHERMFLUSCI.2009.12.010.

[6] Omidi M, Farhadi M, Jafari M. A comprehensive review on double pipe heat exchangers. Appl Therm Eng 2017;110:1075–90. https://doi.org/10.1016/J.APPLTHERMALENG.2016.09.027.

[7] Navickaitė K, Cattani L, Bahl CRH, Engelbrecht K. Elliptical double corrugated tubes for enhanced heat transfer. Int J Heat Mass Transf 2019;128:363–77. https://doi.org/10.1016/J.IJHEATMASSTRANSFER.2018.09.003.

[8] Sheikholeslami M, Gorji-Bandpy M, Ganji DD. Review of heat transfer enhancement methods: Focus on passive methods using swirl flow devices. Renew Sustain Energy Rev 2015;49:444–69. https://doi.org/10.1016/J.RSER.2015.04.113.

[9] Sahin B, Demir A. Thermal performance analysis and optimum design parameters of heat exchanger having perforated pin fins. Energy Convers Manag 2008;49:1684–95. https://doi.org/10.1016/j.enconman.2007.11.002.

[10] Yu C, Zhang H, Wang Y, Zeng M, Gao B. Numerical study on turbulent heat transfer performance of twisted oval tube with different cross sectioned wire coil. Case Stud Therm Eng 2020;22:100759. https://doi.org/10.1016/j.csite.2020.100759.

[11] Tan X, Zhu D, Zhou G, Zeng L. Heat transfer and pressure drop performance of twisted oval tube heat exchanger. Appl Therm Eng 2013;50:374–83. https://doi.org/10.1016/j.applthermaleng.2012.06.037.

[12] Dagdevir T, Ozceyhan V. Investigation of the Effect of Using Water Based Hybrid Nanofluid on Thermal and Hydraulic Performance in a Heat Exchanger. Erciyes Univ J Institue Sci Technol 2021;37:61–73.

[13] Hussein AM, Sharma KV, Bakar RA, Kadirgama K. A review of forced convection heat transfer enhancement and hydrodynamic characteristics of a nanofluid. Renew Sustain Energy Rev 2014;29:734–43. https://doi.org/10.1016/J.RSER.2013.08.014.

[14] Dong X, Jin X, Li P, Bi Q, Gui M, Wang T. Experimental research on heat transfer and flow resistance properties in spiral twisted tube heat exchanger. Appl Therm Eng 2020;176:115397. https://doi.org/10.1016/j.applthermaleng.2020.115397.

[15] Tang X, Dai X, Zhu D. Experimental and numerical investigation of convective heat transfer and fluid flow in twisted spiral tube. Int J Heat Mass Transf 2015;90:523–41